

# Black Holes as Dark Matter Annihilation Boosters

Mattia Fornasa<sup>1,2</sup> and Gianfranco Bertone<sup>2</sup>

<sup>1</sup> *INFN, Sezione di Padova, via Marzolo 8, Padova, Italy and*

<sup>2</sup> *Institut d'Astrophysique de Paris, UMR 7095-CNRS,  
Université Pierre et Marie Curie, 98 bis Boulevard Arago 75014, Paris, France\**

We review the consequences of the growth and evolution of Black Holes on the distribution of stars and Dark Matter (DM) around them. We focus in particular on Supermassive and Intermediate-Mass Black Holes, and discuss under what circumstances they can lead to significant overdensities in the surrounding distribution of DM, thus effectively acting as DM Annihilation Boosters.

## Contents

<b>I. Introduction</b>	1
<b>II. Dark Matter profiles without Black Holes</b>	2
<b>III. Particle density around already-formed Black Holes</b>	3
A. The Fokker-Planck equation and the Bahcall-Wolf solution	3
B. Loss-cone dynamics and BH binaries	8
<b>IV. Adiabatic growth of Black Holes</b>	9
A. Adiabatic growth of Black Holes	9
B. Destruction of spikes	11
C. Regeneration of cusps	12
<b>V. Intermediate Mass Black Holes</b>	13
A. Formation scenarios	13
B. Gamma-rays from DM annihilations around IMBHs	14
C. Contribution of SMBHs and IMBHs to the Gamma-ray Background	16
<b>VI. Conclusions</b>	18
<b>Acknowledgments</b>	20
<b>References</b>	20

## I. INTRODUCTION

To identify the nature of Dark Matter (DM) particles, three different experimental strategies have been devised. First, high-energy colliders like the Large Hadron Collider at CERN [1] may soon be able to produce DM particles, and possibly identify them (see e.g. Refs. [2] and [3] and references therein). Another possibility is *Direct Detection*, based on the search for rare events in which a DM particle scatters off the nuclei of large detectors (see e.g. Ref. [4] for a review). Finally, *Indirect Detection* is based on the search for the products of annihilation or decay of DM particles (such as photons, neutrinos and anti-protons). Many candidates have been proposed for DM, but the most studied ones belong to the class of Weakly Interacting Massive Particles (WIMPs) [5, 6], that includes, among others, the lightest neutralino in Minimal or Non-Minimal Supersymmetric extensions of the Standard Model [7], and the lightest Kaluza-Klein state in models with Unified Extra Dimensions [8, 9, 10].

Here we focus on Indirect DM searches. Ideal targets for Indirect DM searches are nearby, high DM density regions, such as local celestial bodies like the Earth and the Sun, where DM can be captured, or centers of galactic halos (see e.g. Refs. [11, 12, 13, 14, 15, 16, 17]). Two classes of astrophysical objects of particular interest are

---

\*Electronic address: mornasa@pd.infn.it, gianfranco.bertone@iap.fr

SuperMassive Black Holes (SMBHs) [18, 19], with masses from  $10^6$  to  $10^9 M_\odot$  and the more speculative Intermediate Mass Black Holes (IMBHs), with a mass from  $20 M_\odot$  to  $10^6 M_\odot$  (see e.g. Refs. [20, 21, 22] and references therein). Both these classes of compact objects can influence the distribution of DM in which they are embedded, leading to strong overdensities: we review here the impact of the formation and growth of BHs on the surrounding distribution of matter, and the consequences for Indirect DM searches. Being the annihilation flux proportional to the integral of the DM density squared, scenarios where the density is *boosted* by the presence, or the growth, of a central BH, are very promising for Indirect searches. BHs can thus be considered as *DM Annihilation Boosters*.

The paper is organized as follows: in Section II we discuss our current understanding of DM profiles in halos without central BHs. In Section III we address the case of a DM distribution evolving around an already-formed BH. In Section IV, we discuss the case of adiabatic growth and the conditions under which DM “spikes” can form. In Section V we will focus on IMBHs, and show that some of the problems associated to the formation of spikes around SMBHs can be evaded, with important consequences for Indirect DM searches. Conclusions will be drawn in Section VI.

## II. DARK MATTER PROFILES WITHOUT BLACK HOLES

There is strong evidence in favor of the presence of SMBHs at the center of every galaxy with a substantial bulge component [18, 19, 23] and it has been suggested that even globular clusters can harbor IMBHs [20]. Throughout the paper, we will generically refer to large gravitationally bound systems like globular clusters, galaxies and clusters of galaxies, as *galaxies*, and we will refer to their central region as the *nucleus*, which may host BHs. Such compact objects account roughly for  $10^{-3}\%$  of the baryonic mass of the galaxy, which is composed of stars, intergalactic dust and DM. We focus on a generic WIMP scenario, with an annihilation cross section of order  $\sigma v \approx 10^{-26} \text{cm}^3 \text{s}^{-1}$  and a mass ranging between the GeV and the TeV scale.

Since we want to characterize how BHs influence the surrounding distribution of matter, we need to specify how DM is distributed *before* the BHs form, and use this information as initial condition for the problem at hand. Profiles without any central object also receive particular attention *per se*, since the cuspsiness of a DM halo without BH can give informations about the “coldness” of the DM candidate [24]. Recently, *N*-body simulations of galaxies found results in favor of power law profiles (with slope from  $-1$  to  $-1.5$ ) for the nuclear region, emphasizing the contrast with direct observations, such as rotation curves of Low Surface Brightness galaxies (LSBs) [25, 26, 27] and X-ray imaging, which suggest instead the presence of flat DM cores.

Navarro *et al.* [28] and Reed *et al.* [29] used *N*-body techniques to simulate the high resolution evolution of galaxies with masses that go from dwarf galaxies ( $10^{10} M_\odot$ ) to clusters of galaxies ( $10^{15} M_\odot$ ). They fitted the final density profiles with typical parametrizations proposed by Navarro, Frenk and White [30] (NFW):

$$\rho(r) = \frac{\rho_0}{r/r_s(1+r/r_s)^2}, \quad (1)$$

and by Moore [31] (M99):

$$\rho(r) = \frac{\rho_0}{(r/r_s)^{1.5}(1+r/r_s)^{1.5}}, \quad (2)$$

finding that simulated data are well approximated by such profiles, that are, hence, “universal”, in the sense that the same analytical form successfully captures the shape of halos at different masses. However, the logarithmic slope  $\beta(r) = d \ln \rho(r) / d \ln r$  of the density profile decreases faster (more slowly) in the simulated data than does in the NFW (M99) profile at small radii. Moreover, *N*-body simulations do not exhibit any indications that  $\beta(r)$  converges to a central value  $\beta_0$ , as should happen for a NFW profile ( $\beta_0 = -1.0$ ) or for a M99 profile ( $\beta_0 = -1.5$ ). This can be due to the finite resolution of numerical simulations, which can be trusted down to the resolution radius  $r_{min}$ , usually taken to be around 0.5% of the virial radius, depending on the total number of particles in the simulation ( $r_{min} \approx \text{kpc}$ , for Milky Way-sized halos). The structure of the inner region therefore is not clear yet, and the value of the central slope  $\beta_0$  can only be inferred by extrapolation. Since the region near  $r_{min}$  is where the deviations from Eqs. 1 and 2 are stronger, the extrapolation procedure can lead to significant errors.

Aside from these uncertainties, Navarro *et al.* [28] used the density of their simulated halos to state that, given a generic power law profile whose central slope converge to a finite value, such value cannot be steeper than  $-1.5$ . Throughout this paper, we will consider this value as the lower limit for the slope of a DM nuclear profile in absence of BH. The profiles in Eqs. 1 and 2 are particular cases of a more general parametrization, the so-called  $(\alpha, \beta, \gamma)$  profile [32]:

$$\rho(r) = \rho_0 \left(\frac{r_0}{r}\right)^\gamma \frac{1}{[1 + (r/r_0)^\alpha]^{(\beta-\gamma)/\alpha}}, \quad (3)$$

that reduces to  $\rho \propto r^{-\gamma}$  ( $\rho \propto r^{-\beta}$ ) in the limit of small (large) radii, while  $\alpha$  characterizes the sharpness of the change in the logarithmic slope. The NFW is recovered for  $(\alpha, \beta, \gamma) = (1, 3, 1)$  and the M99 for  $(\alpha, \beta, \gamma) = (1, 3, 1.5)$ .

It has been proposed that, for a choice of parameters mimicking the presence of flat cores (e.g. if  $(\alpha, \beta, \gamma) = (2, 3, 0.2)$ ), such profiles provide good fits of both the rotation curves from direct observation of LSB galaxies and of the rotation curves from simulated nuclei, suggesting that core profiles should be preferred to Eqs. 1 and 2 since no contrast between  $N$ -body techniques and observational data is present [33]. A possible explanation for the different results obtained by Navarro *et al.* [28] and Kravtsov *et al.* [33] is the fact that the analysis by Navarro *et al.* does not take into account the large uncertainty in the determination of the luminosity distance of galaxies.

Moreover, it was recently shown [34] that the best fit to simulated data for high-resolution  $\Lambda$ CDM halos is obtained with profiles inspired from the so-called Sérsic law [35]:

$$\ln(\Sigma/\Sigma_e) = -b(X^{1/n} - 1). \quad (4)$$

Such a relation provides the best description of the luminosity profiles of elliptical galaxies and the bulges of disk galaxies [36]:  $\Sigma$  is the projected density,  $X = R/R_e$ , and  $R$  is the projected radius. The parameter  $n$ , called Sérsic index, defines the shape of the profile, and  $b$  is a function of  $n$ , usually chosen so that the radius  $R_e$  contains half of the luminosity of the galaxy.

Eq. 4 can be re-written as

$$\frac{d \ln \Sigma}{d \ln R} = -\frac{b}{n} \left( \frac{R}{R_e} \right)^{1/n}, \quad (5)$$

making explicit the power law behaviour of the logarithm slope. Parametrizing the spatial DM profile in a similar way, we obtain

$$\frac{d \ln \rho(r)}{d \ln r} = -2 \left( \frac{r}{r_{-2}} \right)^{1/n} \quad (6)$$

or  $\rho(r) \approx \exp(-Ar^{1/n})$ , that is called *Einasto profile*, in order to emphasize the difference from the Sérsic law, since we are using now spatial, not projected, quantities.  $r_{-2}$  is the distance from the center where the slope is equal to  $-2$ . Eq. 6 was tested fitting the density of the DM halos simulated by Navarro *et al.* [28], providing better results than a NFW profile, at least for dwarf and galaxy halos [34]. The values of  $n$  (now called the Einasto index), left as a free parameter in the fit, range from 4.33 to 7.44. A more detailed description of this model can be found in Merritt *et al.* [37], where fits to simulated DM halos are studied and compared with alternative parametrizations. A number of recent studies [38, 39] have confirmed that simulated DM density profiles deviate slightly but systematically from the NFW form and are better approximated by Einasto's empirical law.

If the Einasto relation was confirmed as a good parametrization of the inner region of DM halos, this would suggest that a scale-free relation like Eq. 6, describing both dark and luminous matter, is a characteristic feature for systems that form via gravitational clustering.

### III. PARTICLE DENSITY AROUND ALREADY-FORMED BLACK HOLES

#### A. The Fokker-Planck equation and the Bahcall-Wolf solution

A population of particles (both stars and DM particles) around a BH can be described by a distribution function  $f(\mathbf{x}, \mathbf{v}, t)$ , whose evolution is governed by gravitational encounters among particles [40]. In the small-angle approximation, such distribution function slowly diffuses in the phase space  $(\mathbf{x}, \mathbf{v})$  towards a steady-state configuration. The time needed to achieve this equilibrium solution is defined as the relaxation time  $t_{rel}$ . For the stellar population, assuming that all stars have the same mass  $m_*$  [40]:

$$\begin{aligned} t_{rel} &\approx \frac{0.34\sigma^3}{G^2 \rho m_* \ln \Lambda} \\ &\approx 0.95 \cdot 10^{10} \text{ yrs} \left( \frac{\sigma}{200 \text{ km s}^{-1}} \right)^3 \left( \frac{\rho}{10^6 M_\odot \text{ pc}^{-3}} \right)^{-1} \left( \frac{m_*}{M_\odot} \right)^{-1} \left( \frac{\ln \Lambda}{15} \right)^{-1}, \end{aligned} \quad (7)$$

where  $\sigma$  is the velocity dispersion,  $\rho$  the stellar density and  $\ln \Lambda$ , known as the Coulomb logarithm, comes from imposing a physical upper cut-off in the distribution of impact parameters for stellar encounters.  $\ln \Lambda$  is usually

related to the mass of the central BH ( $M_\bullet$ ) expressed in units of stellar masses [41]:

$$\ln \Lambda \approx \ln \left( \frac{r_h \sigma^2}{2Gm_\star} \right) = \ln \left( \frac{M_\bullet}{2m_\star} \right) = \ln(N_\bullet/2). \quad (8)$$

$t_{rel}$  depends on the distance from the center of the galaxy but usually, as in Eqs. 7 and 8, it is computed at the influence radius  $r_h$ , defined as the radius at which the gravitational potential due to the BH is equal to the kinetic energy:

$$r_h = \frac{GM_\bullet}{\sigma^2} \approx 11 \text{ pc} \left( \frac{M_\bullet}{10^8 M_\odot} \right) \left( \frac{\sigma}{200 \text{ km s}^{-1}} \right)^{-2}. \quad (9)$$

In the case a singular isothermal density profile [40] ( $\rho(r) = \sigma/2\pi Gr^2$ ),  $M(r \leq r_h) = 2M_\bullet$ ; and this can be used as an alternative definition of the influence radius. For the Milky Way (MW),  $r_h \approx 3$  pc according to both definitions. There seems to be a clear trend of relaxation times with the mass of the central BH, where smaller objects (corresponding to fainter nuclei) are associated to smaller relaxation times. It can be seen from Fig. 1 (taken from Ref. [23]) using the empirical  $M_\bullet - \sigma$  relation [18]:

$$M_\bullet = 5.72 \cdot 10^6 M_\odot \left( \frac{\sigma}{10 \text{ km s}^{-1}} \right)^{4.86}. \quad (10)$$

Nuclei can then be classified in two different categories. Those nuclei with a relaxation time larger than the Hubble time, cannot have already achieved their relaxed equilibrium configuration, so that their distribution will reflect the process of nuclear formation. They are called *collisionless nuclei*, and they are characterized by a central region with a low density of stars, since near the BH a core is present with a slope  $\lesssim 0.2$  [23], at least for those nuclei where the influence radius is resolved. The “mass deficit” (compared to what one expects from the Sérsic law [35]) is up to 4 times the mass of the central BH. There are, then, galaxies, like the MW and M32 that are characterized by a relaxation time smaller than  $10^{10}$  yrs (at resolved radii, e.g. the MW has  $t_{rel} = 3.5 \times 10^9$  yrs at radius  $\approx 0.1 r_h$ ). These *collisional nuclei* have already reached their steady-state configuration. Usually they are faint nuclei ( $M_V \lesssim -20$ ) and, opposite to cores of collisionless nuclei, the innermost region exceeds the Sérsic law, establishing an inner power law profile with slope steeper than  $\approx 1.5$  or a compact stellar nucleus [42].

In this Section we will restrict ourselves to the case of collisional nuclei where the relaxation time is smaller than the Hubble time and the nucleus has, today, a relaxed, steady-state equilibrium configuration for the stellar population. The diffuse evolution of an isotropic distribution  $f$  is described by the Fokker-Planck equation [40, 41], where gravitational collisions are taken into account and parametrized as:

$$4\pi^2 p(E) \frac{\partial f}{\partial t} = -\frac{\partial F_E}{\partial E} = \frac{\partial}{\partial E} \left[ -D_{EE} \frac{\partial f}{\partial E} - D_E f \right], \quad (11)$$

with

$$D_{EE}(E) = 64\pi^4 G^2 m^2 \ln \Lambda \left[ q(E) \int_{-\infty}^E dE' f(E') + \int_E^0 dE' q(E') f(E') \right], \quad (12)$$

$$D_E(E) = -64\pi^4 G^2 m^2 \ln \Lambda \int_E^0 dE' p(E') f(E'), \quad (13)$$

$$q(E, t) = \frac{1}{3} \int_0^{r_{max}} v^3 r^2 dr = \frac{1}{3} \int_0^{r_{max}} [2(E - \phi)]^{3/2} r^2 dr, \quad (14)$$

while  $p(E) = -\partial q/\partial E$  is the volume of phase-space accessible to stars with energy  $E$ .

The equilibrium solution cannot be a Maxwellian distribution, since it would imply an unphysical stellar density near the BH [44], given that stars cannot be present at radii smaller than the tidal radius  $r_t$ , inside which tidal forces tear stars apart. As a consequence, the distribution function is set to zero for  $r \leq r_t$ .

The physical steady-state solution was determined by Bahcall and Wolf [45], following a previous work of Peebles [46]. They proposed that the equilibrium configuration is a zero-flux solution, and obtained a distribution function with a power-law behaviour  $f(E) \propto |E|^{1/4}$ , with a corresponding power-law density profile  $\rho(r) = \rho_0 r^{-7/4}$ . They also

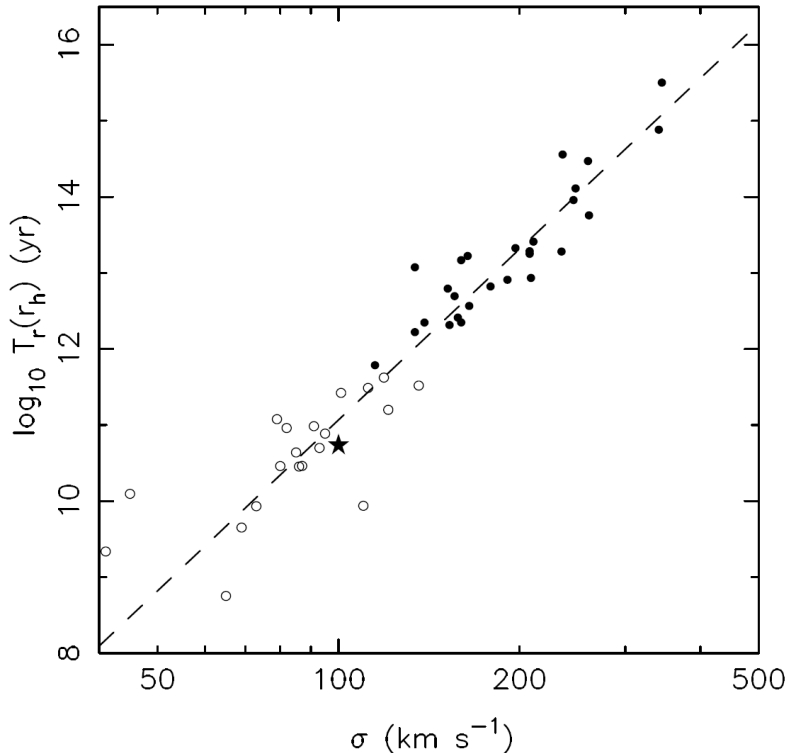


Figure 1: Relaxation times measured at the SMBH influence radius in the ACS/Virgo sample of galaxies (see also Côté *et al.* (2004)), versus the central stellar velocity dispersion. Filled symbols are nuclei in which the influenced radius is resolved. The star is the MW. Figure taken from Merritt (2006).

numerically solved a Fokker-Planck-like equation, obtaining a profile that can be very well described by the zero-flux solution, in the inner region ( $r \lesssim 0.2 r_h$ , where the cusp actually forms), and a Keplerian rise in the velocity dispersion  $\sigma \propto r^{-1/2}$ . See Fig. 2 taken from Ref. [23]. Their solution has been confirmed by  $N$ -body simulations [41], in which the assumptions of isotropy and small-angle, characteristics of the Fokker-Planck-like formalism, had been relaxed.

The validity of Eq. 11 relies on the following assumptions:

- stars are point-like masses, described by a distribution function that evolves due to gravitational interactions with the central BH and among themselves. In particular, this means that encounters in which stars collide with each other are neglected
- the small-angle approximation: the gravitational potential belongs to a particular class of interactions for which the net force experienced by a test particle surrounded by a population of other bodies with which it interacts, is mainly due to cumulative, weak encounters with particles far away, rather than to strong but infrequent interactions with close particles. If we call  $p_0$  the impact parameter for the interaction that causes a deflection of  $45^\circ$  in the velocity of the test particle, all the close encounters with impact parameters  $p \leq p_0$  count only for 4% of the total net deflection [40]. Working under the small-angle approximation means that, in the study of the evolution of a test particle with a velocity  $\mathbf{v}$  embedded in a larger particle population, we are considering only the encounters with those bodies far away that will produce small deflections  $\Delta\mathbf{v}$  compared to the initial velocity  $\mathbf{v}$
- the distribution function does not depend on the angular momentum and, since the gravitational potential is a function only of the radial coordinate, the stellar distribution is isotropic
- the mass of the central BH is much larger than the mass of a star and does not change with time, so that inside the influence radius, the gravitational potential is constant and Keplerian and is due only to the BH itself. Under this assumption we can (as in Eq. 11) neglect the term proportional to  $\partial f / \partial E$  that would appear in a more complete form of the Fokker-Planck equation. Moreover the BH mass has to be much smaller than the total stellar mass near the BH itself. Requiring this particular mass hierarchy [45], leads us to a consequent

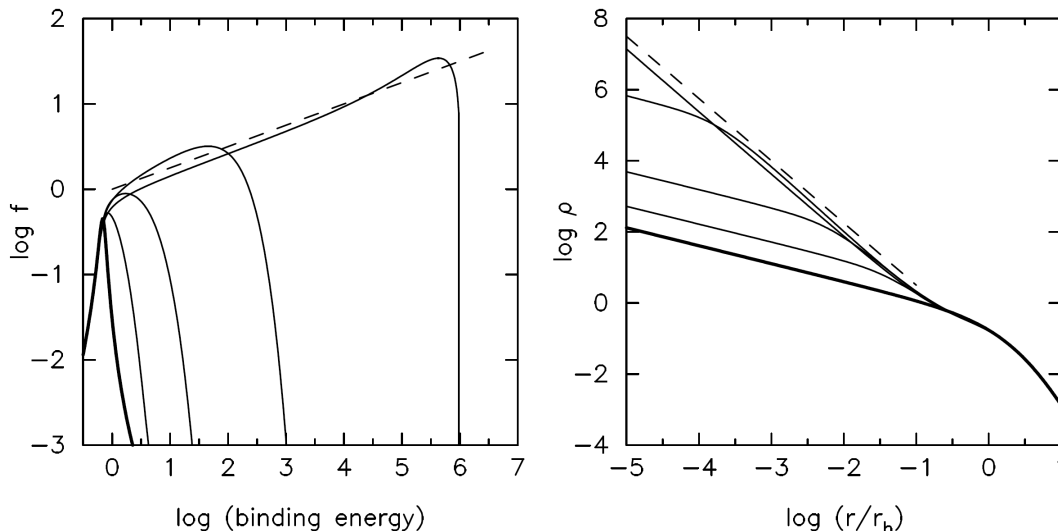


Figure 2: Evolution of the stellar distribution around a SMBH due to energy exchange between stars. These curves were computed from the isotropic, orbit-average Fokker-Planck equation with boundary condition  $f = 0$  at  $\log |E| = 6$ . *Left panel:* phase-space density  $f$ ; *right panel:* configuration-space density  $\rho$ . The initial distribution (shown in bold) had  $\rho \propto r^{-0.5}$  near the SMBH; thin curves show  $f$  and  $\rho$  at times of (0.2, 0.4, 0.6, 1.0) in units of the relaxation time at the SMBH’s initial influence radius  $r_h$ . Dashed line show the “zero-flux” solution  $f \propto |E|^{1/4}$  and  $\rho \propto r^{-7/4}$ . The steady-state density is well approximated by the zero-flux solution at  $r \lesssim 0.2 r_h$ . Figure taken from Merritt (2006).

timescale hierarchy, i.e., the assumption  $m_\star \ll M_\bullet \ll M_\star(r < r_h)$  implies that the crossing time  $t_{cr}$  (the time needed for a star to cross the nucleus) is much shorter than the relaxation time, so that in a crossing time stars do not experience any changes in the physical properties of the system.

All the assumptions listed above can also be satisfied in the case of a distribution of DM particles only (with a common mass  $m_\chi$ ), so that a Fokker-Planck formalism is appropriate also for DM. We expect the existence of a relaxed solution also in this case, but the relaxation timescale for DM is enormously larger than for stars and DM particles will never reach their steady-state solution: they can be effectively considered as collisionless objects, practically not sensitive to the gravitational self-interactions that drive the dynamical evolution described by the Fokker-Planck equation.

The requirement of a common mass for particles (stars or DM) is not included in the list above, because in the more realistic case of a nucleus with particles of different mass, Eq. 11 can be modified in order to describe a multi-mass case. For a two-component nucleus, made of stars (with a common mass  $m_\star$ ) and DM particles with  $m_\chi \ll m_\star$  the Fokker-Planck equations will be the following:

$$4\pi^2 p(E) \frac{\partial g_\star}{\partial t} = \frac{\partial}{\partial E} \left( -m_\star D_{Eg_\star} - D_{EE} \frac{\partial g_\star}{\partial E} \right), \quad (15)$$

$$4\pi^2 p(E) \frac{\partial g_\chi}{\partial t} = \frac{\partial}{\partial E} \left( -D_{EE} \frac{\partial g_\chi}{\partial E} \right), \quad (16)$$

with

$$g_i(E, t) = \int_0^\infty f_i(E, t, m) m \, dm, \quad (17)$$

$$h_i(E, t) = \int_0^\infty f_i(E, t, m) m^2 \, dm, \quad (18)$$

with  $i \in [\star, \chi]$ , and the diffusion coefficients can be written as

$$D_{EE}(E) = 64\pi^4 G^2 m_\star \ln \Lambda \left[ q(E) \int_{-\infty}^E dE' g_\star(E') + \int_E^0 dE' q(E') g_\star(E') \right], \quad (19)$$

$$D_E(E) = -64\pi^4 G^2 \ln \Lambda \int_E^0 dE' p(E') g_\star(E'). \quad (20)$$

$f_\star$  is the stellar distribution function, whose evolution (Eq. 15) is governed by star-star interactions, and  $f_\chi$  is the distribution function for DM and in Eq. 16 only DM-star encounters are considered due to the collisionless nature of DM.

The final steady-state solutions will have the usual  $-7/4$  slope for stars (in fact Eq. 15 is not different from Eq. 11) and a milder  $-3/2$  slope for DM, that will be established in the same timescale  $t_{rel}$  (Eq. 7). The steeping of the initial profile, due to the presence of a BH, leads to an increase of the DM annihilation rate. This is why we refer to BHs as *DM Annihilation Boosters*. Although in this case the effect is not dramatic, since a  $r^{-1.5}$  profile can be found even for models without BHs (see Sec. II), and it is more likely that the overdensity will be reduced in a couple of relaxation times [47] (see Sec. IV C), we will see cases in the next Sections where BHs can provide huge boost factors.

The presence of a stellar cusp has been experimentally confirmed for the MW [48, 49], through the detection of a profile with a slope equal to  $-1.4 < \gamma < -1.3$  in the inner region ( $r \lesssim 0.38$  pc) and to  $-2$  (isothermal profile) in the outer region (see Fig. 3). Our Galaxy is a collisional nucleus, since the relaxation time is shorter than the age of the Universe ( $3.5 \times 10^9$  yrs at  $\approx 0.1 r_h$ ), so it was suggested to interpret its cusp as the Bahcall-Wolf solution to the presence of a SMBH with a mass  $\approx 3.7 \times 10^6 M_\odot$  ( $r_h$  is  $\approx 3$  pc so that the cusp starts more or less where  $r = 0.1 r_h$ ), hypothesis supported also by the luminosity of the X-ray source Sgr A\*. Anyway, it is more likely that the MW experienced a merger between a redshift  $z = 2$  [50] and today, so the cusp will be the result of an “overdensity regeneration” (see Sec. IV C). The actual, detected profile [51] is consistent with a cusp regenerated after a merger occurred at a time  $\gtrsim 8$  Gyr in the past.

The detected inner slope of  $-1.4$  is not exactly what the Bahcall-Wolf solution predicts ( $\gamma = -1.75$ ). However, the two results are considered consistent with each other since the steeper value is derived under the simplifying assumption of a population of stars with identical mass, and if the more realistic multi-mass formalism is introduced, the slope will become shallower, moving towards the  $-1.4$  value. The same can be said if, as it was argued [51], the time required to reach a steady-state solution at the Galactic center is  $\gtrsim 10^{10}$  yr.

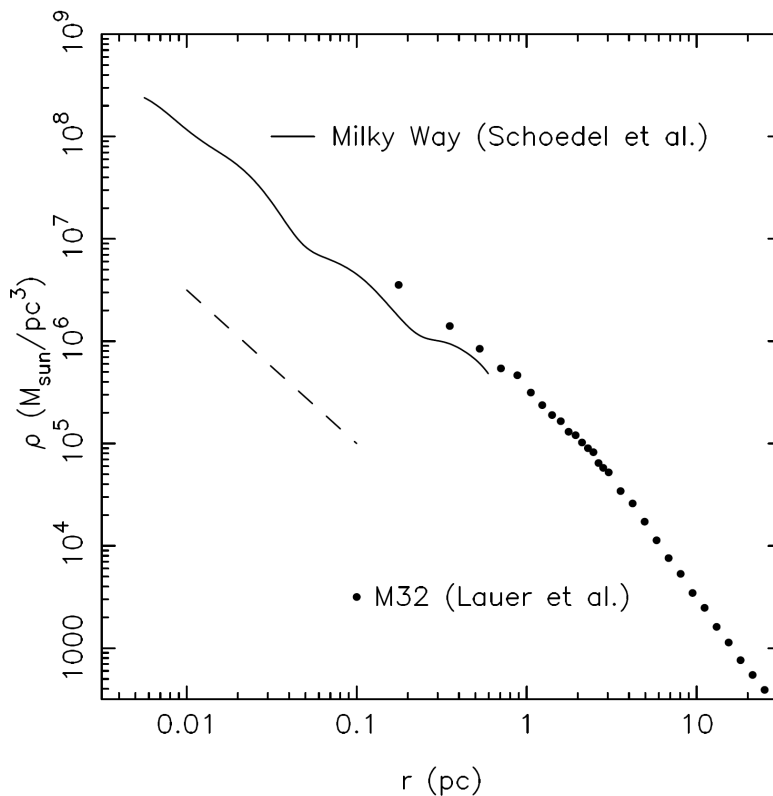


Figure 3: Mass density profiles near the center of the MW and M32. Dashed line is  $\rho(r) \propto r^{-1.5}$ . Both galaxies contain SMBHs with masses  $\sim 3 \cdot 10^6 M_\odot$  and with influence radii  $r_h \approx 3$  pc. Figure taken from Merritt (2006).

## B. Loss-cone dynamics and BH binaries

In this Section, we focus on two mechanisms that can reduce, and even completely destroy, collisional cusps. First of all, we review the basics of *loss-cone* dynamics, i.e. the effects related to the presence of a BH tidal radius or of the relativistic event horizon. This is only partially relevant for DM since it will affect mainly the stellar population, but it is relevant in this context since we have just seen (Eq. 16) how stars and DM evolve together, so that a decrease in the stellar cusp due to loss-cone [23] will influence the DM density, too. Moreover we want to emphasize that any enhancement in the density of DM and stars has to survive to a collection of dynamical mechanisms that can damp them.

After discussing the loss-cone, we will focus on the possibility that, during the merging evolution of a nucleus, a BH binary forms. In this case, both stellar and DM distributions will be directly affected [52], leading not only to the reduction of cusps but also to the possible destruction of spikes in models with adiabatic growth [50] (see Sec. IV B).

The loss-cone of a BH is the set of eccentric orbits populated by stars that are going to intersect the tidal radius. Such orbits are depleted in a crossing time  $t_{cr}$ , since stars are eaten up by the BH: tidal forces inside the tidal radius tear a star apart and these events are accompanied by flares, emissions of light peaked in the X or UV band with a luminosity of  $\approx 10^{44}$  erg s $^{-1}$ . A handful of these flares have been observed: they have the expected signature and the number of detections is roughly consistent with theoretical estimates of the consumption rate  $\dot{N}$  [53, 54, 55, 56].

Once depleted, loss-cone orbits can continue to contribute to the consumption rate only if they are somehow refilled with particles. Energy diffusion provides a mechanism for such a repopulation. In fact,  $N$ -body simulations confirmed [23] that the zero-flux Bahcall-Wolf solution is established only approximately and that (for stars) there is a residual flux  $F(E) \propto r_t^3/t_{rel}(r_t)$ .

This value is too low compared to the expected  $\dot{N}$  whose main contribution comes, instead, from angular momentum diffusion: the “classic loss-cone theory” [45, 57, 58] applies to globular clusters (populated with a central BH), whose relaxation time is so low that they are well-relaxed and old objects. The distribution of stars near the BH is therefore assumed to be on a steady-state, for which a Fokker-Planck-like formalism is appropriate. Resulting estimates for the consumption flux can be introduced in the original Fokker-Planck equation (Eq. 11) to study how particle density is affected by the presence of a tidal radius:

$$4\pi^2 p(E) \frac{\partial f}{\partial t} = -\frac{\partial F_E}{\partial E} + \rho_{lc}(E, t). \quad (21)$$

When extended to the study of galactic nuclei, the steady-state approximation may fail, at least for collisionless nuclei, and the stellar profile near the tidal radius is, in general, different from the Bahcall-Wolf one. For example, galaxies are only approximately spherical: their shape is more likely to be triaxial and there is the possibility that they are governed by centrophilic orbits, i.e. orbits that pass arbitrarily close to the BH. In the case that these chaotic orbits survive until late stages in the galactic evolution,  $\dot{N}$  would increase, since more particles would fall into the tidal sphere.

Alternatively, the present galaxy can be the result of cumulative mergers of less massive mini-galaxies, each of them hosting a mini-BH: the formation of a BH binary would decrease the consumption rate, since all stars with angular momentum  $L \lesssim L_{bin} = (2GM_{12}a_h)$  would be ejected [59] ( $M_{12}$  is the total mass of the binary and  $a_h$  the major semi-axis when the system becomes “hard”), preventing loss-cone repopulation and leading to lower rates  $\dot{N}$ .

Finally, in real galaxies, the diffuse mechanism of orbits refilling will cause the nucleus to expand [23] [60, 61, 62], since the density is reduced when particles are eaten up and those particles which fall into the loss-cone transfer energy to the remaining nucleus with the same effect of a heating process. The expansion is visible in one single relaxation time, the “decay” goes on at a constant velocity and the density can be written as  $\rho(r, t) = \rho_c(t)\rho^*(r)$ , where  $\rho^*(r)$  is the initial profile, while  $\rho_c(t) \propto t^{-1}$ . As a consequence, present-day collisional nuclei could have been denser in the past.

It has been suggested that also the presence of a BH binary can effectively reduce the Bahcall-Wolf cusp. The growth of a galaxy is thought to pass through the agglomeration of smaller galaxies and protogalactic fragments. If more than one of these subhalos contain a BH, the two objects will form a binary system whose dynamics can strongly affect stars and DM. This scenario has received great attention since mergers and the ultimate coalescence of the BH binary are ideal targets for the detection of gravitational waves [63]. Evidences for the presence of such binaries can be found in Ref. [64] and are based on the detection of multiple active nuclei in the same galaxy [65].

Consider a compact object with mass  $M_2$  moving, with its nucleus, around a BH with mass  $M_1$ , being  $q = M_2/M_1 < 1$  the mass ratio and  $M_{12}$  the total mass. The evolution of the binary can be described by three different phases [23, 52]: first, the smaller BH decays due to the dynamical friction with stars of the other nucleus, and the separation  $R_{12}$  between the two objects drops down. When the influence radius  $r_h$  of the more massive BH is reached, the two objects can be considered as a bound object and the first phase comes to an end. The infall time scale [23] suggests



that binaries are not so uncommon since, for reasonable values of  $q$  ( $q \approx 10^{-3}$  and  $M_1 \approx 10^8 M_\odot$ ), they are able to form before the Hubble time.

The second phase is characterized by a quick “shrinking” of the binary, until it becomes *hard*, i.e. the binding energy equals the kinetic energy, or equivalently the major semi-axis reaches [52]  $a_h = q/(1+q)^2 \cdot r_h/4$ . The third phase, when  $a \lesssim a_h$ , is the least known: a binary in a fixed background begins to harden at a constant hardening rate  $s = d(1/a)/dt$ , but physical binaries has already ejected almost all stars on intersecting orbits and the rate suddenly drops. These orbits need to be repopulated, usually by energy diffusion, but this effect is more likely to be only subdominant, at least in those bright galaxies where the scouring of BH binaries has been detected, characterized by a relaxation time higher than the Hubble time. In numerical simulations with finite  $N$ , gravitational encounters will unphysically continue to supply particles to the binary at rates roughly proportional to  $N$ , so experimentally it is more useful to define the semi-major axis  $a_{stall}$  where the hardening rate goes to zero [52]. From  $N$ -body simulations it results

$$\frac{a_{stall}}{r'_h} = 0.2 \frac{q}{(1+q)^2}, \quad (22)$$

$r'_h$  is a second influence radius, defined as the radius where the total mass of particles within  $r'_h$  after the binary has stalled is equal to twice  $M_{12}$ . This values for  $a_{stall}$  is a couple of orders of magnitude higher than the distance where the binary coalescences. This is known as the “final parsec problem”, since evidence is strong that BHs binaries do efficiently coalesce [65, 66] at last. Many solutions have been proposed [67], e.g. that, as for loss-cone orbits, the presence of centrophillic orbits in realistic triaxial galaxies can affect the above considerations, so that the binary continues to shrink even to  $a \lesssim a_h$ .

Assuming that the binary does stall at  $a_{stall}$ , it will have transferred an energy

$$\Delta E \approx -\frac{GM_1 M_2}{2r_h} + \frac{GM_1 M_2}{2a_h} \approx -\frac{1}{2}M_2 \sigma^2 + 2(M_1 + M_2)\sigma^2 \approx 2(M_1 + M_2)\sigma^2, \quad (23)$$

to the particles in the nucleus. This relation has been used to explain the mass deficit in the core of brightest galaxies since such an energy release will let stars leave the central core, with a total displacement of mass  $M_{def}$  and  $0.4 \lesssim M_{def}/M_{12} \lesssim 0.6$  [52] for  $0.05 \lesssim q \lesssim 0.5$ .

Strictly speaking, the observed mass deficits  $M_{def}$  reach values that are even four times larger than the mass of the binary  $M_{12}$  (that, if the coalescence occurs, is also the mass of the final BH). We can account for values as large as  $M_{def}/M_{12} \lesssim 2$  if the nucleus experiences more than one merger, with more than one binary forming. The total mass displaced will be simply the sum of each  $M_{def}$  during each single merger. For even larger values, other mechanisms have to be evoked, e.g. the possibility that a third BH arrives when the first two have not coalesced yet. In such a situation, one of the BH usually leaves the nucleus (*gravitational slingshot* effect) leading to higher values for  $M_{def}$ . Similarly one of the SMBH of a BH binary can be expelled with a high velocity, due to the so-called *gravitational-wave rocket* effect [68].

## IV. ADIABATIC GROWTH OF BLACK HOLES

### A. Adiabatic growth of Black Holes

In this Section we relax the assumption of time-independent gravitational potential. As we will see, this can, in some cases, lead to large DM overdensities. In particular, the adiabatic growth of BHs can produce the steepest DM profiles discussed in literature.

The seed BH grows in an already-formed nucleus with a stable (stellar or DM) configuration. The condition of adiabaticity guarantees that the growth timescale is large compared to the crossing time, but smaller than the relaxation time (for the stellar distribution). As a consequence, nuclei where a BH have grown adiabatically have not yet reached a stable, relaxed stellar configuration. Another consequence [69] is that the angular momentum and the radial action (i.e.  $J_r = \oint v_r dr$ , where  $v_r$  is the radial velocity and the integral is over one closed orbit) are conserved. The hierarchy between the BH accretion timescale and the nuclear crossing time, that lies at the core of the adiabatic assumption, is reasonable at least for BHs with masses  $M_\bullet \lesssim 10^{10} M_\odot$ , as can be checked adopting the shortest timescale for the BH growth, i.e. the Salpeter time  $t_s = M_\bullet / \dot{M}_{Edd}$  (where  $\dot{M}_{Edd}$  is the Eddington accretion rate), and comparing it with the crossing time at the influence radius  $t_{cr} \propto M_\bullet \sigma / r_h$ , using the  $M_\bullet - \sigma$  relation (See Eq. 10).

The first study on the impact of adiabatic growth [70] on stars, analyzed the case of a non-singular isothermal stellar profile, and predicted an overdensity extending to the same size of the initial core, with a slope equal to  $-3/2$ .

In the case of a DM halo, such overdensity has been called *spike* [71], to distinguish it from the aforementioned DM cusps.

A numerical algorithm that mimic adiabatic growth was also developed, in order to confirm the creation of the overdensity [72]. The method is very flexible and, in fact, it was applied to initial models other than the isothermal distribution [72]. Two classes can be identified: the first includes all those profiles called “analytic cores”, characterized by a density that can be expanded in a power law series near the BH ( $\rho(r) \approx \rho_0 + 1/2\rho_0''r^2 + \dots$ ), while the second describes the so-called  $\gamma$  models that exhibit a power law density profile in the inner region:  $\rho(r) \propto r^{-\gamma}$ .

As benchmark cases, the  $\gamma$ -models with  $0 \leq \gamma \leq 2$  and the isothermal model (as an example of analytic profiles) are considered here, and results are presented in Tab. I and in Fig. 4 [73] (only for the isothermal and for  $\gamma = 1$ ).

The spike radius  $r_{sp}$ , i.e. the distance where the slope changes due to the presence of the BH, depends on the BH mass and it is related to the influence radius as  $r_{sp} \approx 0.2 r_h$  [74]. Inside such radius, the spike has a slope  $\gamma_{sp}$ , that depends on the initial  $\gamma$ . In the case of a model with analytic core the final slope is  $-3/2$  [70], while for the  $\gamma$  models an analytic relation holds [46] [72, 75]:

$$\gamma_{sp} = \frac{9 - 2\gamma}{4 - \gamma}. \quad (24)$$

Such relation is valid under the following assumptions (satisfied by all the models in Quinlan *et al.* [72]):

- the distribution function is isotropic;
- the gravitational potential can be written as  $r^{2-\gamma}$  in the  $r \rightarrow 0$  limit;
- $f$  diverges as  $[E - \Phi(0)]^{-n}$  in the limit  $E \rightarrow \Phi(0)$  (this last requirement is what makes a model with analytic core different from a  $\gamma$  model).

Model	$\gamma$	$n$	$\gamma_{sp}$	$C$
isothermal	0	0	3/2	9/4
$\gamma$ model ( $\gamma = 0$ )	0	1	2	9/4
$\gamma$ model ( $\gamma = 1$ )	1	5/2	7/3	7/3
$\gamma$ model ( $\gamma = 3/2$ )	3/2	9/2	12/5	12/5
$\gamma$ model ( $\gamma = 2$ )	2		5/2	5/2

Table I: Different quantities computed from the adiabatic growth of the initial models proposed by Quinlan, Sigurdsson and Hernquist (1995).  $\gamma$  and  $\gamma_{sp}$  are the initial and final slope in the density profile for the region closer to the BH.  $n$  indicates how the distribution function diverges as  $E \rightarrow \Phi(0)$  and  $C$  is the slope of the final density profile if it were made of particles on circular orbits. The value for  $n$  in the  $\gamma = 2$ -model is absent since the equation used to derive  $n$  is not valid for  $\gamma = 2$ , but for  $\gamma \rightarrow 2$  the final profile has  $\gamma_{sp} \rightarrow 5/2$ .

Comparing the first two lines in Tab. I, it can be seen that, even if both models start with a constant core, they develop very different final spikes, due to the different behaviour of the distribution functions in the  $E \rightarrow \Phi(0)$  limit, suggesting that the formation of a strong spike is not a consequence of a singularity in the density profile but in the distribution function, and in particular in the way cold orbits (populated by stars with a low velocity) are arranged (see Sec. IV B). We will not consider initial configurations with  $\gamma$  larger than 1.5 (see Sec. II), so the steepest spike has a slope of  $-12/5$  (when  $\gamma = 1.5$ ).

The velocity dispersion reacts to the BH growth in a similar way for both classes of initial models: in fact, a Keplerian rise appears, with a slope of  $-1/2$ . On the contrary, the anisotropy is substantially different: analytic models exhibit a mild tangential anisotropy at an intermediate distance from the BH but remains isotropic at the center; the more massive the BH is, the higher the anisotropy. While for  $\gamma$  models, orbits are tangentially-biased in the central region and the anisotropic area increases with more massive BHs. If the hypothesis of an isotropic distributions is relaxed, a nucleus made entirely by circular orbits evolves to a profile with final slope equal to  $C$ , shown in Tab. I. As one can see, for  $\gamma$  models  $\gamma_{sp} = C$ , while the circular isothermal model exhibits a much steeper slope, although with a value not higher than for the  $\gamma$  models. Such consideration suggests that results from adiabatic growth are not very sensible to possible violations of isotropy in the initial configuration.

Even if spikes are the steepest known overdensities, they cannot be considered as signatures of BH growing adiabatically (since a simple singular isothermal profile that nothing has to do with adiabatic growth is steeper than half of the models in Tab. I) and neither hints of the presence of a central BH (since a  $-1.5$  slope, as in the first line of Tab. I, can be found for halos without BH). On the contrary, a rise in the  $\sigma$  profile is quite a robust indication of the presence of a central object.

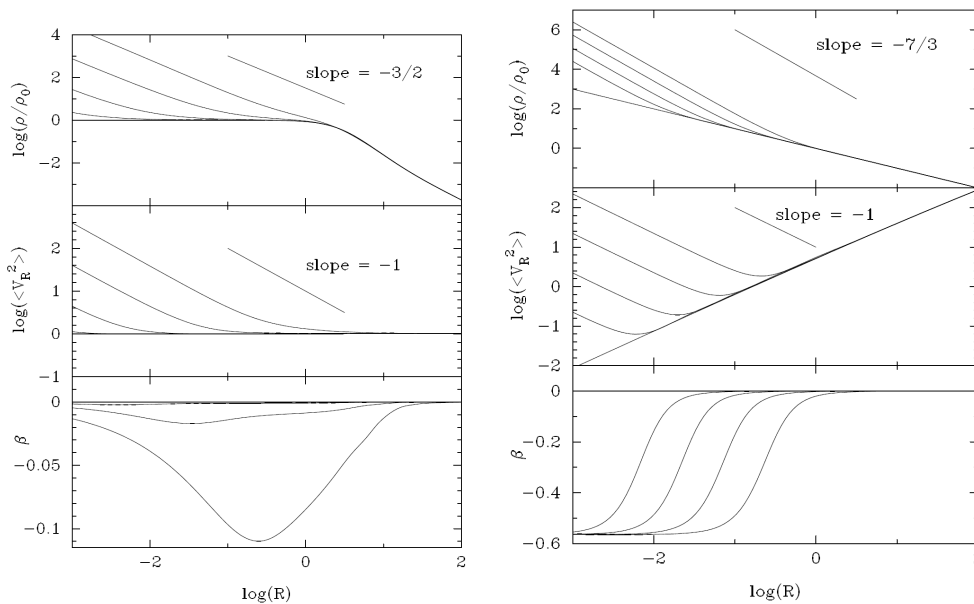


Figure 4: Adiabatic growth in the isothermal (*left panel*) and for a  $\gamma = 1$  (*right panel*) model for a value of  $M_\bullet$  of 0.001, 0.01, 0.1 and 1.0 (mass units explained in the Reference), with the mass increasing from bottom to top in the top two panels and from top to bottom in the last panel. The density is shown in the top frame, the averaged radial velocity in the middle and the anisotropy parameter  $\beta$  in the last frame.  $\beta = 1 - \langle v_t^2 \rangle / \langle 2v_r^2 \rangle$  where  $v_t$  ( $v_r$ ) is the tangential (radial) component of velocity. Figure taken from MacMillan, Henriksen (2002).

## B. Destruction of spikes

The formation of spikes described in the previous Section leads to the largest annihilation boost factors: the mechanism of adiabatic growth can, in fact, produce inner slopes as steep as  $-2.25$  (See Tab. I), for profiles that will be characterized by a large annihilation flux (which is proportional to the integral of the DM density squared), with interesting consequences for Indirect DM searches.

However, it has been argued [75] [50, 76], that the formation of spikes requires *ad hoc* initial conditions for the DM halo. Moreover, even if spikes do form, then, dynamical effects can reduce or even destroy them, as we considered before for collisional cusps. A spike can form even from an initial density profile that does not diverge [75], but in order to produce a significant overdensity, the distribution function of cold orbits has to diverge in the  $E \rightarrow \Phi(0)$  limit. In fact, cold orbits are those which provide the particles that will form the spike, since they are the most affected by the presence of the central BH.

But these cold orbits are more likely to be depleted due to the interactions of stars with molecular clouds or globular clusters or other bodies that can pass through a galactic nucleus. Moreover, the evolution of a galactic nucleus is thought to be characterized by the cumulative mergers of sub-nuclei and even a single merger event can have dramatic consequences on the distribution of cold orbits. In other words, one can enumerate a collection of effects that effectively heat up the particles near the BH, so that they can leave the central region obstructing the formation of the spike.

Also in the case that the spike is formed, it is unlikely that it will survive to the evolution of the nucleus and, in particular to the presence of dynamical mechanisms that would provide an additional heating source to particles on cold orbits, with the result of highly reduce or even destroy the enhancement. Numerical simulations have been performed in order to quantify these effects: for example the possibility that the BH forms slightly off the center of the nucleus was described by Ullio, Zhao and Kamionkowski [75]. The BH would slowly spiral in, towards the center [77], and then adiabatically grow to the final value. But if the initial value for the BH mass is too low, the spiraling would take too long to finally reach the center, while, if the BH is too massive, its scouring effect on the DM particles would flatten the central density, to values that can be even lower than the initial profile (see Fig. 5).

Moreover, gravitational interactions of DM particles with baryons in stars modify the evolution of DM in the spike, reducing the enhancement, in the same way that stars heat the DM particles in a collisional cusp causing its damping (see Sec. IV C) [47] [75]. Simulations on the effects of galactic mergers can also be found in Ref. [50]. Other objections have been put forward, suggesting that spikes can form only as results of a series of accidents and, therefore, are not expected to be common in the local Universe [75].

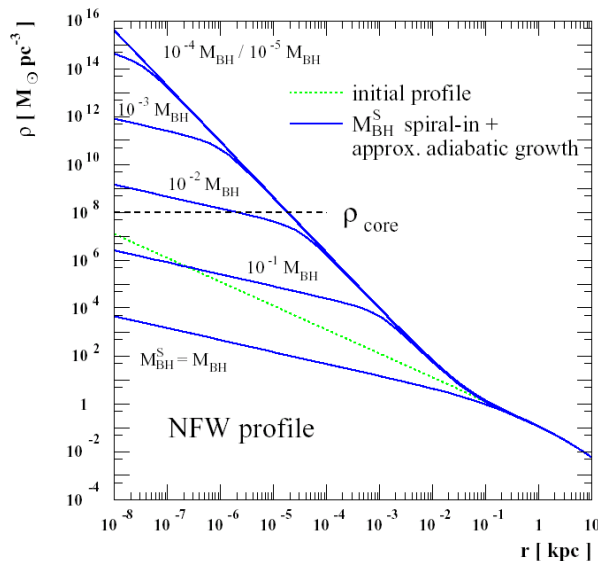


Figure 5: Modification of a NFW DM density profile due to the off-center formation of a BH seed of mass  $M_{BH}^S$ , its spiraling towards the center of the DM distribution, and its adiabatic growth to the present-day mass of the BH  $M_{BH}$  at the Galactic center. Several different values of the BH seed mass are plotted.  $\rho_{core}$  is the maximum WIMP density above which WIMPs are depleted by pair annihilations. Figure taken from Ullio, Zhao and Kamionkowski (2001).

### C. Regeneration of cusps

In the previous Sections we focused on processes that can destroy overdensities (whether cusps or spikes). However, gravitational interactions among particles (during the evolution of the nucleus) can partially regenerate such structures. In a realistic nucleus populated by stars and DM, star-star collisions and star-DM collisions (given enough time) drive the evolution towards a steady-state  $-7/4$  profile for the baryonic component and a  $-3/2$  profile for the DM component [47] (see Section III A). This is true also if the nucleus is the result of an early evolution phase in which previous enhancements were destroyed. In other words, consider a nucleus with a short  $t_{rel}$  and a steep DM and stellar profile (due to collisional relaxation or adiabatic growth of the central BH). If a merger occurs and a BH binary forms, the displaced mass will reduce or even destroy both overdensities. But, due to the short relaxation time, it can happen that the nucleus has enough time to reconstruct, from the core profile after the BHs coalescence, the collisional solutions. The new DM cusp is called CREST (Collisionally REgenerated STructure). This idea can be checked analytically, applying the two-body Fokker-Plack formalism to a core profile describing a nucleus after the scouring of a BH binary, but also with the help of numerical routines [47]. Results are summarized in Fig. 6: DM CRESTs are not as steep as spikes, but they have the advantage to form from very general initial profiles, given that the (stellar) relaxation time is short enough. They need a timescale of roughly  $t_{rel}(0.2 r_h)$  to form, but then DM particles in the CREST continue to be heated by gravitational interactions with stars and the  $-3/2$  solution, therefore, decays in a self-similar way

$$\rho_\chi(r, t) \approx \rho_{\chi,0}(r)G(t/t_{rel}), \quad (25)$$

with  $dG/dt < 0$ , so that after  $4.5 t_{rel}(r_h)$  the reduction is of a factor  $1/e^2$ .

The balance between the requirement that the relaxation time is short enough to let the CREST form but not too short to make the CREST not to decay too much, leaves us with a rather narrow window of galaxies where CRESTs can be present: one can detect them in galaxies with a luminosity  $3 \cdot 10^8 L_\odot \lesssim L \lesssim 3 \cdot 10^9 L_\odot$ . The MW is inside this range and, in fact, many proposed to interpret the cusp detected for our Galaxy [49] as a reconstructed structure after a merger occurred  $\sim 8$  Myr ago [51].

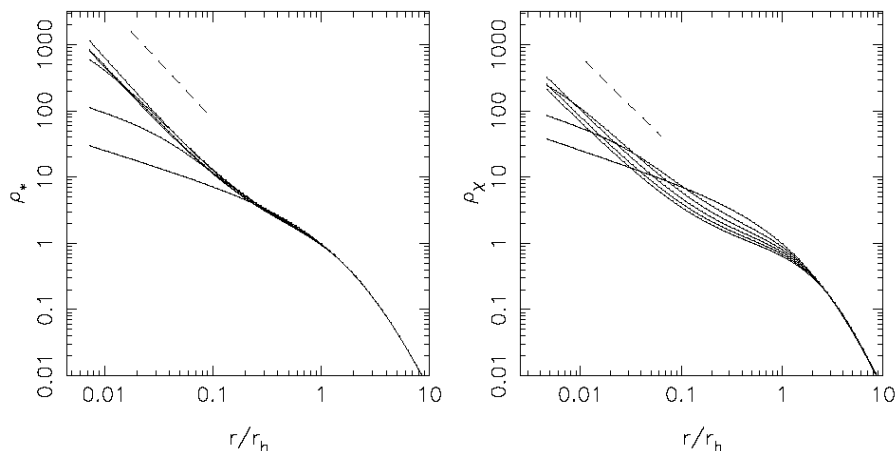


Figure 6: Solutions of the Fokker-Planck equation that describe the joint evolution of stars and dark matter around a BH due to star-star and star-DM gravitational encounters. Length unit is  $r_s$ , while the density is in units of the initial value at  $r_h$ . Curves show the stellar (left) and DM (right) density profiles at time 0, 0.2, 0.4, 0.6, 0.8, 1.0 in units of the initial relaxation time at  $r_h$ . Dashed lines are the steady-state solutions. Figure taken from Merritt, Harfst and Bertone (2006).

## V. INTERMEDIATE MASS BLACK HOLES

### A. Formation scenarios

The steep DM slopes produced by the adiabatic growth of BHs make these objects extremely interesting since they may effectively act as DM Annihilation Boosters. This circumstance encouraged many authors to look for possible ways to evade the dynamical effects causing spikes to damp.

Two possibilities have been proposed: the first is to focus on IMBHs instead than of SMBHs. IMBHs can be present within substructures of DM halos [20, 21] and their evolution is such that the objections raised for spikes around SMBHs do not apply [22]. The second is considering the contribution of spikes and mini-spikes (DM overdensity around IMBHs) to the diffuse Extragalactic Gamma ray Background (EGB), integrating the signal from high redshift, i.e. when spikes were already formed but destruction mechanisms were not yet effective [78, 79, 80].

We focus on IMBHs first. Their masses range from  $\approx 20$  to  $10^6 M_\odot$  and adiabatic growth leads to the formation of “mini-spikes” in the same way as with SMBHs. We don’t have direct observational evidence for the existence of IMBHs, but some hints come, e.g., from Ultra Luminous X-ray sources (ULXs) [81], sources that emit in the X band with a luminosity higher than  $10^{39} \text{erg s}^{-1}$ , and, hence, not compatible with the interpretation as BHs accreting at the Eddington limit. But, due to their positions in the host galaxy, they cannot be explained in terms of AGNs either. The hypothesis of a BH with a mass higher than  $15 - 20 M_\odot$  and less massive than a SMBH seems to be a fair explanation, instead.

Many authors also proposed that globular clusters can host IMBHs, and a possible confirmation of this hypothesis comes from the fact that the mass scale for an IMBH and the value of the stellar velocity dispersion measured in globular clusters fall exactly at the extrapolation at lower values of the  $M_\bullet - \sigma$  relation valid for SMBHs [20]. From a theoretical point of view, IMBHs can also help to explain the formation of SMBHs: the Sloan Digital Survey [82] [83, 84] has detected quasars up to redshift  $z \approx 6$  suggesting that SMBHs were already present when the Universe was  $\sim 1$  Gyr old. One of the most natural way to understand this is that SMBHs grew, through a phase of fast accretion and mergers, starting from already massive seeds. In fact, a generic prediction of scenarios that seek to explain the properties of the observed SMBH population, is that a large number of “wandering” IMBHs exist in DM halos [85, 86] [21].

Despite their theoretical interest, it is difficult to obtain conclusive evidence for the existence of IMBHs. A viable detection strategy could be the search for gravitational waves produced in the mergers of the IMBHs population [63, 87, 90, 91], with space-based interferometers such as the Large Interferometric Space Antenna LISA [92].

Two formation scenarios are discussed here, following Ref. [22]. In the first (scenario A), IMBHs form from the gravitational collapse of Population III stars, which are usually heavier than local stars, since they grow in an environment with very low metallicity, for which metal line cooling can be neglected. As a consequence, the Jeans mass (that scales with the temperature as  $T^{3/2}$ ) is higher, allowing the formation of more massive structures. Such stars are characterized by very low metallicity, too, meaning that they will lose little of their mass due to winds and

weak pulsations. Population III stars with masses above larger than  $250M_\odot$  would be able to collapse directly to BHs without any explosion [20].

In the second scenario (scenario B), the formation starts at high redshift ( $z \approx 15$ ) from a gas cloud that is massive enough to cool down forming a protogalactic pressure-supported disc at the center of the cloud, made mainly by stars that, according to the distribution of angular momentum in the cloud, are in the low momentum tail of the distribution. The dynamics of the disc is governed by an effective viscosity that transfers matter at the center and angular momentum outward. This flow will go on until the first stars start to fragment in the outer region of the disc: the so-formed central object will undergo gravitational collapse, forming the final BH, with a mass scale of  $\approx 10^5 M_\odot$  (corresponding to an initial cloud with virial mass  $M_{vir} \approx 10^7 M_\odot$ ) or [22]

$$M_\bullet = 3.8 \times 10^4 M_\odot \left(\frac{\kappa}{0.5}\right) \left(\frac{f}{0.03}\right)^{3/2} \left(\frac{M_{vir}}{10^7 M_\odot}\right) \times \left(\frac{1+z_f}{18}\right)^{3/2} \left(\frac{t}{10 \text{ Myr}}\right), \quad (26)$$

where  $f$  is the fraction of the total baryonic mass in the gas cloud that has cooled into the disc,  $\kappa$  is that fraction of the baryonic mass of the disc that forms the final BH,  $M_{vir}$  is the halo virial mass,  $z_f$  is the redshift when the formation starts from the cloud and  $t$  the timescale for the evolution of the first generation of stars.

Regardless of the particular formation scenario, a population of IMBHs is predicted, each of them surrounded by a mini-DM halo and a mini-spike. These mini-halos evolve, merge with each other and form the actual big halos of galaxies. The hosted IMBHs will merge too, possibly contributing to the formation of the central SMBH. However a fraction of initial mini-halos never experiences any mergers and the associated DM overdensity can survive till today.

Moreover, at least for scenario B, IMBHs form exactly at the center of the baryonic distribution in the mini-halos, forbidding BH off-center formation. Strictly speaking, in order to avoid off-center formation, one should require that the pristine BH forms at the center of the DM distribution and this does not necessarily coincide with the center of baryons, since stars, been collisional, can experience a different evolution than the collisionless DM, resulting in a net displacement between the two distributions. But mini-halos are supposed to have a very low baryonic content, with no violent interactions able to drive the two distributions away one from the other: the fact that mini-halos are made most entirely by DM solves the possible off-center formation and, at the same time, the problem related to stars-DM interactions. Scenario B is thus able to circumvent all the mechanisms for spike destruction described above, while in scenario A they are reduced but still efficient: in the following Sections, we are going to consider scenario A as a conservative model for IMBHs, instead of the more optimistic scenario B.

For the MW, an IMBHs population of  $1027 \pm 84$  objects is predicted by the numerical simulations in Ref. [22], with a mass of approximatively  $10^2 M_\odot$  (scenario A), while for the scenario B the MW hosts just  $101 \pm 22$  with a distribution in mass centered on  $10^5 M_\odot$  and log-normally distributed ( $\sigma_\bullet = 0.9$ ), as it can be seen in the left panel of Fig. 7.

## B. Gamma-rays from DM annihilations around IMBHs

The prospects for indirect detection of DM from mini-spikes around IMBHs populating the MW halo has been studied by Bertone, Zentner and Silk [22]. They considered 200 different statistical realizations of the MW, obtaining an IMBH catalogue where each object is surrounded by a mini-DM halo with an inner slope of  $-7/3$ , resulting from adiabatic growth of an initial NFW profile (Eq. 1).

The spike extends from a *cut radius*  $r_{cut}$  to the outer spike radius  $r_{sp} \approx 0.2 r_h$ . The cut radius depends on the mass and annihilation cross section of the DM candidate, being defined as the radius where the DM density reaches an upper limit due to DM annihilations [22].

Eq. 27 was used to compute the annihilation flux from each mini-spike:

$$\begin{aligned} \Phi &= \int_{E_{thr}}^{m_\chi} dE \frac{d\Phi(E)}{dE} \\ &= \int_{E_{thr}}^{m_\chi} dE \frac{1}{2} \frac{\sigma v}{m_\chi^2} \frac{1}{d^2} \frac{dN_\gamma}{dE} \int_{r_{cut}}^{r_{sp}} \rho_{sp}^2(r) r^2 dr, \\ &= \Phi_0 \frac{dN_\gamma}{dE} \left(\frac{\sigma v}{10^{-26} \text{cm}^3 \text{s}^{-1}}\right) \left(\frac{m_\chi}{100 \text{ GeV}}\right)^{-2} \left(\frac{d}{\text{kpc}}\right)^{-2} \\ &\quad \cdot \left(\frac{\rho(r_{sp})}{10^2 \text{ GeV cm}^{-3}}\right)^2 \left(\frac{r_{sp}}{\text{pc}}\right)^{14/3} \left(\frac{r_{cut}}{10^{-3} \text{ pc}}\right)^{-5/3}, \end{aligned} \quad (27)$$

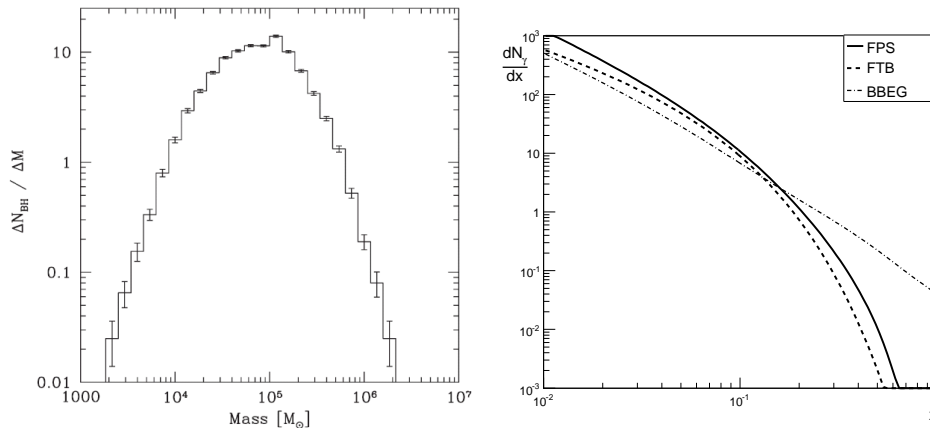


Figure 7: *Left panel:* Mass function of unmerged IMBHs in scenario B, for a MW halo at  $z = 0$ , averaged over 200 Monte Carlo realizations of a MW-like halo with virial mass  $M_{vir} = 10^{12.1} h^{-1} M_{\odot}$ . Figure taken from Bertone, Zentner and Silk (2005). *Right panel:* Differential photon spectrum per annihilation. Different parametrizations and annihilation channels are shown. The solid line is an analytic fit to the  $b\bar{b}$  channel, as obtained by Fornengo, Pieri and Scopel (2004) with  $m_{\chi} = 1$  TeV. The dashed line is relative to the same annihilation channel, but with a different parametrization of the Fragmentation Functions obtained by Fornasa, Taoso and Bertone (2007). The dotted line is relative to UED DM and includes FSR from annihilation to charged leptons. Figure taken from Fornasa, Taoso and Bertone (2007).

where  $\Phi_0 = 9 \cdot 10^{-10} \text{cm}^{-2} \text{s}^{-1}$ ,  $m_{\chi}$  is the mass of the DM particle and  $\sigma v$  its thermally-averaged annihilation cross section.  $d$  is the distance of the IMBH from the detector and  $dN_{\gamma}/dE$  is the number of photons with energy from  $E$  to  $E + dE$  produced by the annihilation. The differential flux is then integrated in energy from a lower threshold  $E_{th}$  that depends on the experiment considered, up to  $m_{\chi}$ .

The differential spectrum  $dN_{\gamma}/dE$  can be written as a sum over all possible annihilation channels of the number of photons  $dN_{\gamma}^a/dE$  produced from the particular channel  $\chi\chi \rightarrow a\bar{a}$ , weighted by the corresponding branching ratio  $B^a = \text{BR}(\chi\chi \rightarrow a\bar{a})$ :

$$\frac{dN_{\gamma}}{dE} = \sum_a B^a \frac{dN_{\gamma}^a}{dE}. \quad (28)$$

If DM particles annihilate directly into photons, the spectrum will be a line at an energy equal to the DM particle mass, but this contribution is usually suppressed at least for a neutralino-like DM candidate (a branching ratio to primary photons of  $\approx 10^{-3}$  is used in Ref. [79]). Otherwise the spectrum will be a continuum, and we can distinguish between two classes of spectra: in the first one photons are produced from the decay of neutral pions ( $\pi^0 \rightarrow \gamma\gamma$ ) formed through the fragmentation of annihilations products such as heavy quarks, gauge or Higgs bosons. Many parametrizations are available for these spectra  $dN_{\gamma}/dE$  [93] [94, 95], that represent a suitable approximation for neutralino-like candidates. In the right panel of Fig. 7, two possible examples for the fragmentations of the neutral pion  $\pi^0$  are compared [93, 95], in the easy-to-consider case of DM annihilating only to a pair of  $b$  quarks [22].

The second possibility is inspired from candidates arising in theories with Universal Extra-Dimensions, where the DM can annihilate to charged leptons with a large branching ratio (for neutralinos, such channel is severely suppressed). Such final states, then, can produce photons through the so-called Final State Radiation (FSR). A typical FSR spectrum is plotted in Fig. 7 with a 40% of DM annihilating to light fermions, 20% to  $\tau\tau$  and the remaining in  $b$  quarks. The photon production through light fermions is computed analytically [96] while the other two channels are described as in the NPD spectrum.

Differences between the two classes of annihilation spectra become more pronounced above  $x \approx 0.6$ , since at low energy the pion decay dominates. The FSR spectrum is characterised by a flatter spectrum (the slope is approximately  $-1$  instead of  $-1.5$  for NPD decay) and by a more abrupt cut-off at an energy equal to the DM particle mass.

The prospects for detecting IMBHs in the MW are summarized in Fig. 8 where the number of point-like sources (associated to IMBHs) with an annihilation flux higher than  $\Phi$ , is plotted as a function of  $\Phi$ . Compared with the sensitivities of GLAST [97] (a Space-Based telescope scheduled to be launched at the beginning of 2008) and EGRET [98] (a Space-Based gamma-ray detector, whose data are available on Ref. [99]) for a  $5\sigma$  detection, the most optimistic configuration ( $m_{\chi} = 100$  GeV and  $\sigma v = 3 \cdot 10^{-26} \text{cm}^3 \text{s}^{-1}$ ) leads to almost 100 (80) detectable sources by GLAST (EGRET) in 1 year.

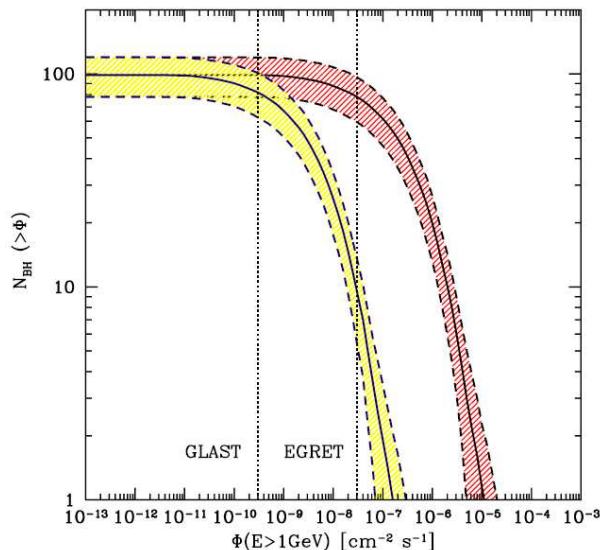


Figure 8: IMBHs integrated luminosity function, i.e. number of BHs producing a gamma-ray flux larger than a given flux, as a function of the flux, for scenario B and a NPD spectrum. The upper (lower) line corresponds to  $m_\chi = 100$  GeV,  $\sigma v = 3 \cdot 10^{-26} \text{ cm}^3 \text{ s}^{-1}$  ( $m_\chi = 1$  TeV,  $\sigma v = 10^{-29} \text{ cm}^3 \text{ s}^{-1}$ ). For each curve we also show the  $1\sigma$  scatter among different realization of the MW DM halo. The figure can be interpreted as the number of IMBHs that can be detected from experiments with a point-source sensitivity  $\Phi$  (above 1 GeV), as a function of  $\Phi$ . We show for comparison the  $5\sigma$  point-source sensitivity above 1 GeV of EGRET and GLAST (1 year). Figure taken from Bertone, Zentner and Silk (2005).

The prospects for Indirect DM detection usually strongly depend on the particle physics parameters. For IMBHs, however, the  $\sigma v/m_\chi^2$  dependence of the flux in Eq. 27 is modified by the implicit dependence of the cut radius on the mass  $m_\chi$  and the annihilation cross section  $\sigma v$ , so that at the end  $d\Phi/dE \propto (\sigma v)^{2/7} m_\chi^{-9/7}$ .

In order to discriminate IMBHs from other extragalactic sources, one can perform a maximum likelihood analysis of the annihilation spectrum or look for a class of sources with an identical cut-off, at the mass of the DM particle [22]. Alternatively, one may look at the Andromeda galaxy M31 [95], which is located  $\approx 780$  kpc away from us, and where a population of  $65 \pm 15$  objects (in scenario B) is predicted. A fraction of these BHs ( $17 \pm 6$  for  $m_\chi = 150$  GeV with a NPD spectrum) can be detected with GLAST. In this case, the DM signature will be the detection of up to 20 point-like, bright, gamma-ray sources in a  $3^\circ$  circle around the Andromeda center (see Fig. 9).

### C. Contribution of SMBHs and IMBHs to the Gamma-ray Background

EGRET data have shown the existence of an Extragalactic diffuse Gamma-ray Background (EGB) in the GeV range [100, 101], initially interpreted as photons from an unresolved population of blazars [102]. Today such astrophysical sources are believed to play a significant role but they can hardly account for the entire background, while DM spikes and mini-spikes could in principle strongly contribute to the flux.

Ullio *et al.* [103] estimated the contribution of DM annihilations from halos without central BHs to the EGB. The total number of photons that contributes to the EGB from redshift  $z$  is in this case:

$$dN_\gamma = \int dM(1+z)^3 \frac{dn}{dM}(M, z) \frac{\sigma v}{2m_\chi^2} \frac{dN_\gamma(E)}{dE} \cdot \int d\mathbf{r} \rho^2(\mathbf{r}, M, z) e^{-\tau(E_0, z)} \frac{dV dA}{4\pi(R_0 r)^2} dE_0 dt_0, \quad (29)$$

where  $dn/dM$  is the comoving number density of DM halos with mass  $M$  at redshift  $z$  and it is computed using the Press-Schechter formalism [80, 104]. The  $(1+z)^3$  factor converts comoving to proper density, while  $dN_\gamma/dE$  is the usual annihilation spectrum described in the last Section.  $\rho$  is the DM density and the factor  $e^{-\tau(E_0, z)}$  takes into account the gamma ray absorption due to pair production with the ExtraGalactic Background Light in the infrared



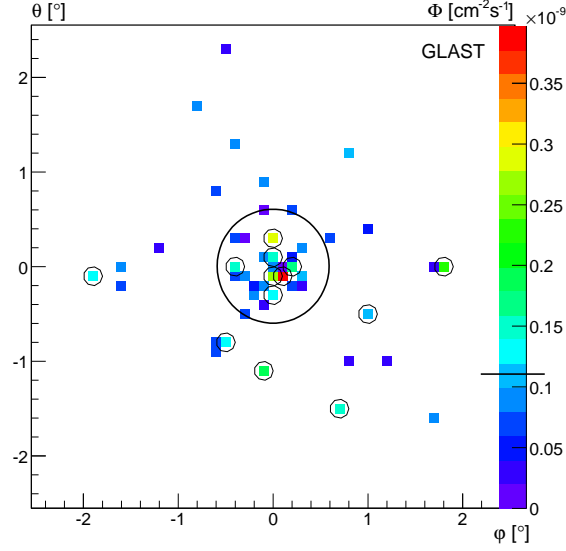


Figure 9: Map of the gamma-ray flux, in units of photons  $\text{cm}^{-2}\text{s}^{-1}$ , from DM annihilations around IMBHs in M31, relative to one random realization of IMBHs in M31. The size of the bins is  $0.1^\circ$  and the energy threshold is 4 GeV, as appropriate for GLAST. The big circle shows, for comparison, the M31 scale radius  $r_s$ , and the small circles highlight IMBHs within the reach of GLAST ( $5\sigma$  detection in 2 months). Figure taken from Fornasa, Taoso and Bertone (2007).

or optical band ( $\tau \approx (E_0/10 \text{ GeV})^{0.8}(z/3.3)$ ).  $E_0$  is the energy today so that  $dEdt = dE_0(1+z)dt_0(1+z)^{-1}$  and  $R_0$  is the today scale factor.

Each halo is described by a NFW (Eq. 1) or M99 (Eq. 2) profile, whose concentration parameter  $c$  ( $c = r_{vir}/r_s$ ) depends on redshift as in Eke, Navarro and Steinmetz [105]. In order to reproduce the EGRET diffuse flux, a large boost factor would be required, that, if applied to the Galactic center, would grossly exceed the EGRET measurement of the gamma ray flux from Sgr A\* [80].

The presence of a spike would only marginally affect the signal from the Galactic center, because even if the spike was present in the past for the SMBH of the MW, it would already be destroyed. However, for the EGB spikes are indeed important, since the background receives contributions from halos at high redshift, at a time when astrophysical and particle physics effects did not have time yet to damp DM overdensities [78].

Ahn *et al.* [78] included spikes around SMBHs in the computation made by Ullio *et al.*. The authors used the phenomenological relation between the mass of the BH  $M_\bullet$  and the mass of the hosting halo  $M_h$  [106]:  $M_\bullet/10^8 M_\odot = a(M_h/10^{12} M_\odot)^b$ , where  $M_h$  is considered at  $z = 0$  and different values for  $(a, b)$  are used [78].

For each halo at  $z = 0$ , a SMBH with mass  $M_\bullet$  (related to  $M_h$ ) is posed at the redshift of BH formation  $z = z_\bullet$  and the halo is evolved till now (assuming that  $M_h$  remains unchanged). The spikes form and then decay in a self-similar way (see Section IV C,  $\rho(r, t) \approx \rho(r, 0)\kappa = \rho(r, 0)e^{-\tau/2}$ ), so that the evolution of the spike is described by

$$\rho_{sp}(r, t) = \rho_{sp,0} \kappa^\epsilon \left( \frac{r}{r_{s,0}} \right)^{-\gamma_{sp}}, \quad (30)$$

with  $\gamma$  and  $\gamma_{sp}$  are the slopes of the initial and final profile,  $\epsilon = (\gamma_{sp} - \gamma)^{-1}$  and  $\tau$  is the time since spike formation in units of the heating time  $t_{heat}$ :

$$t_{heat} = 1.25 \text{ yr} \cdot \left( \frac{M_\bullet}{3 \cdot 10^6 M_\odot} \right)^{1/2} \left( \frac{r_h}{2 \text{ kpc}} \right)^{3/2} \left( \frac{m_\star}{M_\odot} \right)^{-1} \left( \frac{\ln \Lambda}{15} \right)^{-1}. \quad (31)$$

If we specify a NFW profile for the DM density before the spike formation, the complete DM distribution can be written as follows:

$$\begin{cases} \rho(r)_{NFW} & (z > z_\bullet) \\ \rho(r)_{NFW} & (z \leq z_\bullet, r > r_{s,0}) \\ \rho(r)_{NFW} + \rho_{sp}(r, t) \approx \rho_{sp}(r, t) & (z \leq z_\bullet, r \leq r_{s,0}) \end{cases}. \quad (32)$$

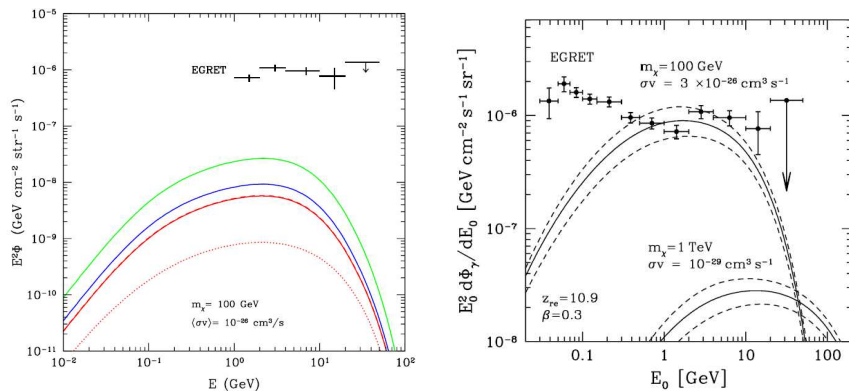


Figure 10: *Left*: Gamma-ray background produced by DM annihilations in DM halos with spikes (solid lines), compared to the halo-only contribution (dotted). The EGRET diffuse flux limits are shown for comparison. Three choices for the parameters in the relation between the mass of the BH and the mass of the halo are used:  $(a, b) = (0.027, 1.82)$  in red,  $(0.10, 1.65)$  in blue and  $(0.67, 1.82)$  in green. The DM parameters adopted are  $m_\chi = 100$  GeV,  $\sigma v = 10^{-26} \text{ cm}^3 \text{ s}^{-1}$ . Figure taken from Ahn, Bertone, Merritt and Zhang (2007) *Right*: Contribution to the EGB from scenario A and scenario B IMBH mini-spikes. Also shown are the EGRET data and predictions for the case of standard halos without spikes and mini-spikes. The  $1\sigma$  scatter in the number of IMBHs is shown for scenario A. For scenario B, the  $1\sigma$  scatter for the number of IMBHs and for the upper limit in the redshift integration are shown combined. Results are shown for  $m_\chi = 100$  GeV and  $\sigma v = 3 \cdot 10^{-26} \text{ cm}^3 \text{ s}^{-1}$ . Figure taken from Horiuchi and Ando (2006).

For a DM particle of 100 GeV the contribution to the EGB is summarized in the left panel of Fig. 10, that shows an enhancement of more than an order of magnitude with respect to the case without SMBHs. The main contribution comes from low-energies, due to the annihilations at high redshift in the still-present spikes. The energy of the produced photons is then redshifted till now.

The EGB from DM annihilation in mini-spikes around IMBHs has been calculated in Ref. [79]. The results are shown in the right panel of Fig. 10 for a neutralino of 100 GeV and both the formation scenarios. As before, the main contribution is at low energies, but now the predictions from scenario B are able to account for all the EGB, and the same is true if one consider the line spectrum. This model is sensitive to the average of the halos properties, whereas, in the case of annihilation e.g. from the Galactic Center, one has to deal with a single realization that may differ significantly from the average, so that the study of gamma ray background and the way DM contributes is, for Indirect searches, an interesting alternative to the study of unidentified sources.

## VI. CONCLUSIONS

We have reviewed the consequences of the growth and evolution of BHs on the distribution of stars and DM around them. Initially, the BH mass was considered to be fixed in time, with particles evolving around it under the influence of its gravitational potential and their gravitational collisions. A steady-state solution is predicted for stars only for collisional nuclei: it is a zero-flux solution characterized by a central cusp with a slope of  $-7/4$  [45] within  $0.2 r_h$ . DM particles, being collisionless, are not affected by self gravitational interactions but by encounters with stars [47]: in the same time that the  $-7/4$  cusp forms for stars, the DM distribution is rearranged in a profile with a central slope of  $-3/2$ , that will decay due to heating. Other effects can significantly reduce collisional overdensities, e.g. both stellar and DM cusps react to the presence of a BH binary [52] and the stellar number density can be influenced by loss-cone dynamics [23].

In the case of adiabatic growth of a BH, instead, the final DM and stellar overdensities are much steeper, reaching slope as large as  $-2.25$  [71, 72]. But again, the evolution of the host galaxy drives a suppression of the spike, due to cumulative mergers [50] and possible off-center BH formation [75]. Even if DM overdensities around BHs may seem to be very promising for Indirect detection, the presence of spikes is probably not realistic [75]. Alternative strategies include the study of DM contribution to the EGB and the search for IMBHs. In the first case, the gamma-ray background receives contribution from BHs at high redshift, when spikes and mini-spikes were already present, but damping mechanisms were not effective yet. DM annihilations from spikes around SMBHs at high redshift contribute significantly to the EGB [78]. A population of IMBHs is then able to reproduce the value detected by EGRET, even for standard assumptions for the initial DM profile [79].

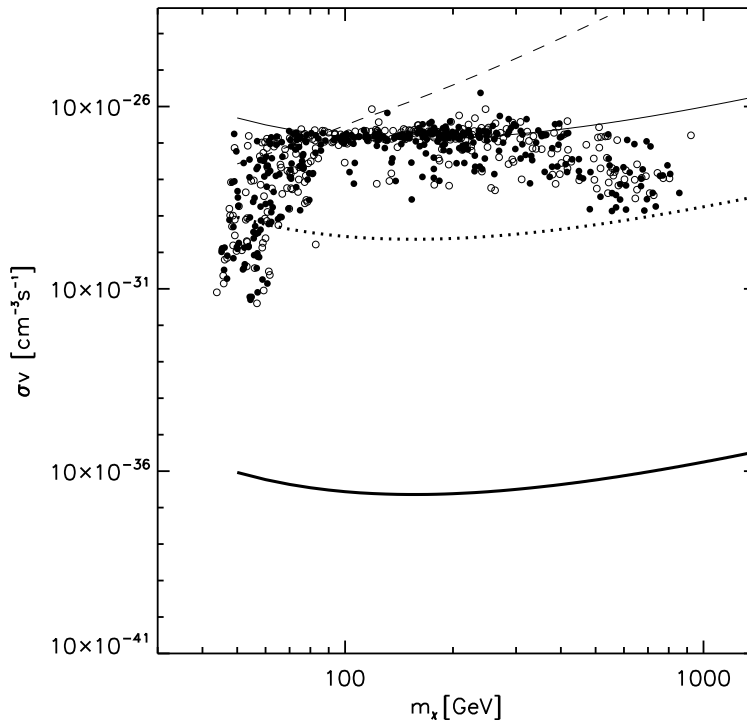


Figure 11: Exclusion plot in the DM mass vs. annihilation cross section plane. Above the thick (dotted) solid line all the statistical realizations of a MW-like halo in Bertone, Zentner and Silk (2005) contain at least one IMBH with an annihilation flux larger than the estimated point source sensitivity of GLAST (EGRET) in 2 months. Above the thin solid line all the statistical realizations of the Andromeda galaxy in Fornasa, Taoso and Bertone (2007) have at least one IMBH with an annihilation flux larger than  $10^{-10} \text{cm}^{-2} \text{s}^{-1}$ . The dotted line indicates the region above which the contribution from DM annihilation around IMBHs at high redshift can account for the EGB as measured by EGRET. The empty (full) dots represent SUSY models (obtained with DarkSusy) where the neutralino relic density is within 3 (5) $\sigma$  from the WMAP-measured value.

Mini-spikes around IMBHs can effectively be searched for with GLAST and can be identified with a careful spectral analysis of the signal [22]. They can also be searched for in the Andromeda galaxy, distributed in a quite characteristic fashion that leaves no room for alternative astrophysical interpretations [95].

We show in Fig. 11 the constraining power of the different detection strategies discussed above:

- the dotted and solid lines are relative to the population of IMBHs in our Galaxy [22]. For each value of the mass of the DM candidate, we estimate the value of  $\sigma v$  for which all the aforementioned realizations of the Milky Way have *at least one* IMBH that should have been detected by EGRET at  $5\sigma$ , as discussed in Ref. [22]. In other words, if none of the EGRET unidentified sources can be interpreted as IMBH, a model with a combination  $(m_\chi, \sigma v)$  above the dotted line is compatible with the data with a probability less than 0.5%. The solid line shows the prospectesd for detection with GLAST
- the thin solid line is relative to the population of IMBHs in M31 [95]. For each value of  $m_\chi$  we determined the value of  $\sigma v$  for which all the 200 realizations of M31 have at least one IMBH with an annihilation flux larger than the  $5\sigma$  sensitivity of GLAST (parametrized as in Ref. [95]), for an exposure of 2 months, and an energy threshold of 4 GeV. Null searches of IMBHs in Andromeda will exclude the region above the thin line
- the dashed line is relative to the contribution of IMBHs to the EGB [79]. Each point above the line corresponds to a DM candidate for which annihilations in IMBHs mini-spikes at high redshift exceeds the EGB values as measured by EGRET in Ref. [100].
- the empty dots represent Supersymmetric Models (generated with DarkSusy [107]) for which the neutralino can account for all the DM, being within  $3\sigma$  from the WMAP determination of the DM relic density [108]
- the full dots represent SUSY Models within  $5\sigma$  from WMAP

GLAST can thus probe regions of the parameter space at very low cross section, so that IMBHs can be soon discovered or ruled out. If none of these sources is detected by GLAST, it is very unlikely than such scenario will survive, at least for a WIMP DM candidate.

The gamma-ray flux from DM annihilations in spikes and mini-spikes has been widely discussed in literature (Refs. [12, 47, 50, 71, 75, 76, 109], just to name a few) and many experimental collaborations are actively working to improve their discovery potential. But so far, the gravitational effects of BHs have only been observed through their impact on stellar populations, since there is not a detected signal currently and clearly interpreted as DM annihilation. Photons from DM annihilations could have been detected in the past as subdominant contributions from gamma-ray sources [11] but the main challenge remains to disentangle such a contribution from other photon production mechanisms.

Instead, the effect of a central BH on the stellar population has been detected for the MW [48, 49] and such interpretation is proposed also for other galaxies of the Local Group [110, 111], encouraging further attempts of detecting BH effects on DM and, eventually, of detecting DM indirectly through its annihilations products.

### Acknowledgments

We thank David Merritt for many useful comments and suggestions.

- 
- [1] <http://lhc.web.cern.ch/lhc/>.
  - [2] E. A. Baltz, M. Battaglia, M. E. Peskin and T. Wizanski, Phys. Rev. D **74** (2006) 103521 [arXiv:hep-ph/0602187].
  - [3] A. K. Datta, K. Kong and K. T. Matchev, Phys. Rev. D **72** (2005) 096006 [arXiv:hep-ph/0509246].
  - [4] C. Munoz, Int. J. Mod. Phys. A **19** (2004) 3093 [arXiv:hep-ph/0309346].
  - [5] G. Bertone, D. Hooper and J. Silk, Phys. Rept. **405** (2005) 279 [arXiv:hep-ph/0404175].
  - [6] L. Begström, Rept. Prog. Phys. **63** (2000) 793 [arXiv:hep-ph/0002126].
  - [7] G. Jungman, M. Kamionkowski and K. Griest, Phys. Rept. **267** (1996) 195 [arXiv:hep-ph/9506380].
  - [8] T. Appelquist, H.-C. Cheng and B. A. Dobrescu, Phys. Rev. D **64** (2001) 035002 [arXiv:hep-ph/0012100].
  - [9] G. Servant and T. M. P. Tait, Nucl. Phys. B **650** (2003) 391 [arXiv:hep-ph/0206071].
  - [10] H.-C. Cheng, K. T. Matchev and M. Schmaltz, Phys. Rev. D **66** (2002) 056006 [arXiv:hep-ph/0205314].
  - [11] F. Aharonian *et al.* [H.E.S.S. collaboration], Phys. Rev. Lett. **97** (2006) 221102 [arXiv:hep-ph/0610509].
  - [12] G. Zaharijas and D. Hooper, Phys. Rev. D **73** (2006) 103501 [arXiv:astro-ph/0603540].
  - [13] S. Profumo, Phys. Rev. D **72** (2005) 103521 [arXiv:astro-ph/0508628].
  - [14] Y. Mambrini, C. Munoz, E. Nezri and F. Prada, JCAP **0601** (2006) 010 [arXiv:hep-ph/0506204].
  - [15] G. Bertone and D. Merritt, Mod. Phys. Lett. A **20** (2005) 1021 [astro-ph/0504422].
  - [16] A. Cesarini, F. Fucito, A. Lionetto, A. Morselli and P. Ullio, Astropart. Phys. **21** (2004) 267 [arXiv:astro-ph/0305075].
  - [17] A. Bouquet, P. Salati and J. Silk, Phys. Rev. D **40** (1989) 3168.
  - [18] L. Ferrarese and H. Ford, Space Science Review **116** (2005) 523 [arXiv:astro-ph/0411247].
  - [19] J. Kormendy and L. C. Ho (2000) [astro-ph/0003268].
  - [20] M. C. Miller and E. J. M. Colbert, Int. J. Mod. Phys. D **13** (2004) 1 [arXiv:astro-ph/0308402].
  - [21] S. M. Koushiappas, J. S. Bullock and A. Dekel, Mon. Not. Roy. Astron. Soc. **354** (2004) 292 [arXiv:astro-ph/0311487].
  - [22] G. Bertone, A. Zentner and S. M. Koushiappas, Phys. Rev. D **72** (2005) 103517 [arXiv:astro-ph/0509565].
  - [23] D. Merritt, Rep. Prog. Phys. D **69** (2006) 2513 [arXiv:astro-ph/0605070].
  - [24] S. Tremaine and J. Gunn, Phys. Rev. Lett. **42** (1979) 407.
  - [25] W. J. G. de Blok and A. Bosma, Astronomy and Astrophysics **385** (2002) 816.
  - [26] W. J. G. de Blok, Astrophys. J. **634** (2005) 227 [arXiv:astro-ph/0506753].
  - [27] G. Gentile, A. Burkert, P. Salucci, U. Klein and F. Walter, Astrophys. J. **634** L145 [arXiv:astro-ph/0510607].
  - [28] J. F. Navarro, E. Hayashi, C. Power, A. Jenkins, C. S. Frenk, S. D. M. White, V. Springel, J. Stadel and T. R. Quinn, Mon. Not. R. Astron. Soc. **349** (2004) 1039 [arXiv:astro-ph/0311231].
  - [29] D. Reed, F. Governato, L. Verde, J. Gardner, T. Quinn, J. Stadel, D. Merritt and G. Lake, Mon. Not. R. Astron. **357** (2005) 82 [arXiv:astro-ph/0312544].
  - [30] J. F. Navarro, C. S. Frenk and S. D. M. White, Astrophys. J. **490** (1997) 493.
  - [31] B. Moore, T. Quinn, F. Governato, J. Stadel and G. Lake, Mon. Not. R. Astron. Soc. **310** (1999) 1147 [arXiv:astro-ph/9903164].
  - [32] H. S. Zhao, Mon. Not. R. Astron. **278** (1996) 488 [arXiv:astro-ph/9509122].
  - [33] A. V. Kravtsov, A. A. Klypin, J. S. Bullock and J. R. Primack, Astrophys. J. **502** (1998) 48 [arXiv:astro-ph/9708176].
  - [34] D. Merritt, J. F. Navarro, A. Ludlow and A. Jenkins, Astrophys. J. **624** (2005) L85 [arXiv:astro-ph/0502515].
  - [35] J. L. Sérsic, *Atlas de galaxias australes* (1968), Cordoba, Argentina: Observatorio Astronomico.
  - [36] A. W. Graham and R. Guzmán, Astrophys. J. **125** (2003) 2936 [arXiv:astro-ph/0303391].
  - [37] D. Merritt, A. W. Graham, B. Moore, J. Diemand and B. Torzic, Astron. J. **132** (2006) 2685 [arXiv:astro-ph/0509417].
  - [38] L. Gao, J. F. Navarro, S. Cole, C. Frenk, S. D. M. White, V. Springel, A. Jenkins and A. F. Neto, astro-ph/0711.0746.

- [39] E. Hayashi and S. D. M. White, astro-ph/0709.3933.
- [40] L. Spitzer Jr., *Dynamical Evolution of Globular Clusters*, Princeton Series in Astrophysics (1987), Princeton, New Jersey.
- [41] M. Preto, D. Merritt, R. Spurzem, *Astrophys. J.* **613** (2004) L109 [arXiv:astro-ph/0406324].
- [42] P. Côte, S. Piatek, L. Ferrarese, A. Jordàn, D. Merritt, E. W. Peng, M. Hasegan, J. P. Blajeslee, S. Mei, M. J. West, M. Milosavljević and J. L. Tonry, *Astrophys. J. Suppl.* **165** (2006) 57.
- [43] P. Côte, J. P. Blakeslee, L. Ferrarese, A. Jordan, S. Mei, D. Merritt, M. Milosavljević, E. W. Peng, J. L. Tonry and M. J. West, *Astrophys. J. Suppl.* **153** (2004) 223 [arXiv:astro-ph/0404138].
- [44] S. L. Shapiro, S. A. Teukolski, *Black Holes, White Dwarfs and Neutron Stars, the physics of compact objects*, John Wiley & sons (1983).
- [45] J. N. Bahcall, R. A. Wolf, *Astrophys. J.* **209** (1976) 214.
- [46] P. J. E. Peebles, *Gen. Rel. and Grav.*, **3** (1972) 63.
- [47] D. Merritt, S. Harfst and G. Bertone, *Phys. Rev. D* **75** (2007) 043517 [arXiv:astro-ph/0610425].
- [48] R. Genzel, R. Schödel, T. Ott, F. Eisenhauer, R. Hofmann, M. Lehnert, A. Eckart, T. Alexander, A. Sternberg, R. Lenzen, Y. Clénet, F. Lacombe, D. Rouan, A. Renzini and L. E. Tacconi-Garman, *Astrophys. J.* **594** (2003) 812 [arXiv:astro-ph/0305423].
- [49] R. Schödel, A. Eckart, T. Alexander, D. Merritt, R. Genzel, A. Sternberg, L. Meyer, F. Kul, J. Moultaqa, T. Ott and C. Straubmeier [astro-ph/0703178].
- [50] D. Merritt, M. Milosavljević, L. Verde and R. Jimenez, astro-ph/0201376.
- [51] D. Merritt and A. Szell, *Astrophys. J.* **648** (2006) 890 [arXiv:astro-ph/0510498].
- [52] D. Merritt, *Astrophys. J.* **648** (2006) 976 [arXiv:astro-ph/0603439].
- [53] S. Komossa (2002) [astro-ph/0209007].
- [54] S. Komossa, J. Halpern, N. Schartel, G. Hasinger, M. Santos-Lleo and P. Predehl, *Astrophys. J.* **603** (2004) L17 [arXiv:astro-ph/0402468].
- [55] J. P. Halpern, S. Gezari and S. Komossa, *Astrophys. J.* **604** (2004) 572 [arXiv:astro-ph/0402497].
- [56] J.-X. Wang and D. Merritt, *Astrophys. J.* **600** (2004) 149 [arXiv:astro-ph/0305493].
- [57] J. Frank and M. J. Rees, *Mon. Not. R. Astron.* **176** (1976) 633.
- [58] H. Cohn and R. M. Kulsrud, *Astrophys. J.* **226** (1978) 1087.
- [59] D. Merritt and J.-X. Wang, *Astrophys. J.* **621** (2005) L101 [arXiv:astro-ph/0411210].
- [60] M. Freitag, P. Amaro-Seoane and P. Kalogera, *Astrophys. J.* **649** (2006) 91 [arXiv:astro-ph/0603280].
- [61] B. W. Murphy, H. N. Cohn and R. H. Durisen, *Astrophys. J.* **370** (1991) 60.
- [62] H. Baumgardt, J. Makino and T. Ebisuzaki, *Astrophys. J.* **613** (2004) 1143 [arXiv:astro-ph/0406231].
- [63] K. S. Thorne and V. B. Braginskii, *Astrophys. J.* **204** (1976) L1.
- [64] S. Komossa, V. Burwitz, G. Hasinger, P. Predehl, J. S. Kaastra and Y. Ikebe, *Astrophys. J.* **582** (2003) L15 [arXiv:astro-ph/0212099].
- [65] C. Rodriguez, G. B. Taylor, R. T. Zavala, A. B. Peck, L. K. Pollack and R. W. Romani, *Astrophys. J.* **646** (2006) 49 [arXiv:astro-ph/0604042].
- [66] D. Merritt and L. Ferrarese, *Mon. Not. R. Astron. Soc.* **320** (2001) L30 [arXiv:astro-ph/0009076].
- [67] A. Gualandris and D. Merritt, astro-ph/0708.3083
- [68] A. Gualandris and D. Merritt, astro-ph/0708.0771.
- [69] J. Binney and S. Tremaine *Galactic Dynamics* (1987) Princeton, Princeton Univ. Press.
- [70] P. Young, *Astrophys. J.* **242** (1980) 1232.
- [71] P. Gondolo and J. Silk, *Phys. Rev. Lett.* **83** (1999) 1719 [arXiv:astro-ph/9906391].
- [72] G. D. Quinlan, L. Hernquist and S. Sigurdsson, *Astrophys. J.* **440** (1995) 554.
- [73] J. D. MacMillan and R. N. Henriksen, *Astrophys. J.* **569** (2002) 83 [arXiv:astro-ph/0201153].
- [74] D. Merritt, Proceedings of Carnegie Observatories Centennial Symposium *Coevolution of Black Holes and Galaxies* [arXiv:astro-ph/0301257].
- [75] P. Ullio, H. S. Zhao, M. Kamionkowski, *Phys. Rev. D* **64** (2001) 043504 [arXiv:astro-ph/0101481].
- [76] G. Bertone and D. Merritt, *Phys. Rev. D* **72** (2005) 103502 [arXiv:astro-ph/0501555].
- [77] T. Nakano and J. Makino, *Astrophys. J.* **525** (1999) L77.
- [78] E.-J. Ahn, G. Bertone, D. Merritt, P. Zhang [arXiv:astro-ph/0703236].
- [79] S. Horiuchi and S. Ando, *Phys. Rev. D* **74** (2006) 103504 [arXiv: astro-ph/0607042].
- [80] S. Ando, *Phys. Rev. Lett.* **94** (2005) 171303 [arXiv:astro-ph/0503006].
- [81] D. A. Swartz, K. K. Ghosh, A. F. Tennant and K.-W. Wu [arXiv:astro-ph/0405498].
- [82] X. Fan *et al* [SDSS Collaboration], *Astron. J.* **122** (2001) 2833 [arXiv:astro-ph/0108063].
- [83] A. J. Barth, P. Martini, C. H. Nelson and L.C. Ho, *Astrophys. Lett.* **594** (2003) L95.
- [84] C. J. Willott, R. J. McLure and M. J. Jarvis, *Astrophys. J.* **587** (2003) L15 [arXiv:astro-ph/0303062].
- [85] R. Islam, J. Taylor and J. Silk, *Mon. Not. Roy. Astron. Soc.* **340** (2003) 6471 [arXiv:astro-ph/0208189].
- [86] M. Volonteri, F. Haardt, and P. Madau, *Astrophys. J.* **582** (2003) 559 [arXiv:astro-ph/0207276].
- [87] É É Flanagan and S. A. Hughes, *Phys. Rev. D* **57** (1998) 4566.
- [88] É É Flanagan and S. A. Hughes, *Phys. Rev. D* **57** (1998) 4535.
- [89] R. Islam, J. Taylor and J. Silk, *Mon. Not. Roy. Astron. Soc.* **354** (2004) 629 [arXiv:astro-ph/0309559].
- [90] T. Matsubayashi, H. Shinkai and T. Ebisuzaki, *Astrophys. J.* **614** (2004), 864.
- [91] S. M. Koushiappas and A. R. Zentner, arXiv:astro-ph/0503511.

- [92] <http://lisa.nasa.gov/>.
- [93] N. Fornengo, L. Pieri, S. Scopel, Phys. Rev. D **70** (2004) 103529 [arXiv:hep-ph/0407342].
- [94] G. Bertone, G. Servant and G. Sigl, Phys. Rev. D **68** (2003) 044008 [arXiv:hep-ph/0211342].
- [95] M. Fornasa, M. Taoso and G. Bertone [astro-ph/0703757].
- [96] L. Bergström, T. Bringmann, M. Eriksson and M. Gustafsson, Phys. Rev. Lett. **94** (2005) 131301 [arXiv:astro-ph/0410359].
- [97] <http://www-glast.stanford.edu>.
- [98] <http://coss.gsfc.nasa.gov/docs/cgro/egret/>.
- [99] <ftp://legacy.gsfc.nasa.gov/compton/data/egret/>.
- [100] P. Sreekumar *et al.* [EGRET collaboration], Astrophys. J. **494** (1998) 523 [arXiv:astro-ph/9709257].
- [101] A. W. Strong, I. V. Moskalenko and O. Reimer, Astrophys. J. **613** (2004) 956 [arXiv:astro-ph/0406254].
- [102] T. Narumoto and T. Totani, Astrophys. J. **643** (2006) 81 [arXiv:astro-ph/0602178].
- [103] P. Ullio, L. Bergstrom, J. Edsjö, C. G. Lacey, Phys. Rev. D **66** (2002) 123502 [arXiv:astro-ph/0207125].
- [104] W. Press and P. Schechter, Astrophys. J. **187** (1974) 425.
- [105] V. R. Eke, J. F. Navarro and F. Steinmetz, Astrophys. J. **554** (2001) 114 [arXiv:astro-ph/0012337].
- [106] L. Ferrarese, Astrophys. J. **578** (2002) 90 [arXiv:astro-ph/0203469].
- [107] <http://physto.se/~edsjo/darksusy/>.
- [108] D.N. Spergel *et al.* (WMAP collaboration), Astrophys. J. Suppl. **170** (2007) 377 [arXiv:astro-ph/0603449].
- [109] L. Pieri and E. Branchini, Phys. Rev. D **69** (2004) 043512 [arXiv:astro-ph/0307209].
- [110] T. R. Lauer, S. M. Faber, D.G. Currie, S. P. Ewald, E. J. Groth, J. J. Hester, J. A. Holtzman, R. M. Light, E. J. O'Neil Jr., E. J. Shaya and J. A. Westphal, Astrophys. J. **104** (1992) 552.
- [111] P. J. Young, J. A. Westphal, J. Kristian, C. P. Wilson and F. P. Landauer, Astrophys. J. **221** (1978) 721.